Familial Alzheimer mutations stabilize synaptotoxic γ-secretase-substrate complexes

Sujan Devkota[1,†], Rui Zhou[2,†], Vaishnavi Nagarajan[1,†], Masato Maesako[3], Hung Do[4,‡], Arshad Noorani[1], Caitlin Overmeyer[5], Sanjay Bhattarai[1], Justin T. Douglas[6], Anita Saraf[7], Yinglong Miao[4,8], Brian D. Ackley[8], Yigong Shi[2,9], and Michael S. Wolfe[1,5,10*]

[1]Department of Medicinal Chemistry, University of Kansas, Lawrence, KS, USA

[2] Beijing Frontier Research Center for Biological Structure, Tsinghua-Peking Joint Center for Life Sciences, School of Life Sciences, Tsinghua University, Beijing, China.

[3]Alzheimer Research Unit, MassGeneral Institute for Neurodegenerative Disease, Massachusetts General Hospital, Harvard Medical School, Boston, MA, USA

[4]Center for Computational Biology, University of Kansas, Lawrence, KS, USA

[5]Graduate Program in Neurosciences, University of Kansas, Lawrence, KS, USA

[6]Nuclear Magnetic Resonance Core Lab, University of Kansas, Lawrence, KS, USA

[7]Mass Spectrometry and Analytical Proteomic Laboratory, University of Kansas, Lawrence, KS, USA

[8]Department of Molecular Biosciences, University of Kansas, Lawrence, KS, USA

[9]Westlake Laboratory of Life Science and Biomedicine; Key Laboratory of Structural Biology of Zhejiang Province, School of Life Sciences, Westlake University; and Institute of Biology, Westlake Institute for Advanced Study, Hangzhou, Zhejiang Province, China

[10]Lead Contact:

[†]These authors contributed equally to the study

[‡]Current affiliation: Theoretical Division, Los Alamos National Laboratory, Los Alamos, NM, USA

[*] mswolfe@ku.edu

SUMMARY

Mutations that cause familial Alzheimer's disease (FAD) are found in amyloid precursor protein (APP) and presenilin, the catalytic component of γ-secretase, that together produce amyloid β-peptide (Aβ). Nevertheless, whether Aβ is the primary disease driver remains controversial. We report here that FAD mutations disrupt initial proteolytic events in the multi-step processing of APP substrate C99 by γ-secretase. Cryo-electron microscopy reveals that a substrate mimetic traps γ-secretase during the transition state, and this structure aligns with activated enzyme-substrate complex captured by molecular dynamics simulations. *In silico* simulations and *in cellulo* fluorescence microscopy support stabilization of enzyme-substrate complexes by FAD mutations. Neuronal expression of C99 and/or presenilin-1 in *Caenorabditis elegans* leads to synaptic loss only with FAD-mutant transgenes. Designed mutations that stabilize the enzyme-substrate complex and block Aβ production likewise led to synaptic loss. Collectively, these findings implicate the stalled process—not the products—of γ-secretase cleavage of substrates in FAD pathogenesis.

Key words: Proteolysis, cryoelectron microscopy, protein structure, molecular dynamics, fluorescence microscopy, *C. elegans*, neurodegeneration

INTRODUCTION

The discovery of dominant missense mutations in APP associated with familial Alzheimer's disease (FAD) led to original formulation in 1991 of the amyloid hypothesis of Alzheimer's disease pathogenesis,[1,2] which posits that aggregation of secreted Aβ peptides, particularly the 42-residue variant Aβ42, leads to a cascade of events culminating in neurodegeneration and dementia. Subsequent findings that presenilins are sites of FAD mutations that alter Aβ production, are essential for γ-secretase processing of APP to Aβ, and comprise the catalytic component of the γ-secretase complex provided strong support for the amyloid hypothesis.[3] Nevertheless, the assembly state of neurotoxic Aβ and associated signaling pathways remain unclear,[4] and clinical candidates targeting Aβ or its aggregates have shown little or no benefit in the prevention or treatment of Alzheimer's disease,[5,6] the recent approval of anti-Aβ monoclonal antibodies notwithstanding,[6,7] raising doubts about Aβ as a major driver of the disease process.

The pathology, presentation and progression of FAD are closely similar to those of the more common sporadic late-onset Alzheimer's disease,[8,9] and the dominantly inherited monogenic nature of FAD suggests that elucidation of pathogenic mechanisms should be more tractable. Because dominant missense FAD mutations are only found in the substrate and the enzyme that produce Aβ, such mutations all likely lead to altered proteolytic processing of APP substrate by γ-secretase. However, this processing is complex, with the APP transmembrane domain (TMD) cleaved multiple times by the membrane-embedded γ-secretase complex to produce Aβ peptides along two pathways: Aβ49→Aβ46→Aβ43→Aβ40 and Aβ48→Aβ45→Aβ42→Aβ38 (Figure 1A).[10] We recently reported comprehensive analysis of effects on each of these proteolytic events for 14 FAD mutations in the APP TMD, finding that every mutation was deficient in the first or second carboxypeptidase trimming step, elevating levels of Aβ peptides of 45 residues and longer.[11] Such complete and quantitative analysis has not been reported for any presenilin FAD mutations.

Here we expand the analysis of each proteolytic processing step of C99 by γ-secretase to elucidate effects of FAD mutations in presenilin-1 (PSEN1), revealing consistent deficiencies in initial processing steps, not later steps that produce secreted forms of Aβ such as Aβ42. An atomic-resolution structure of the active γ-secretase complex bound noncovalently with a full transmembrane substrate mimetic provides a snapshot of the enzyme at or near the transition state, as it would be when poised for intramembrane proteolysis. This new structure in turn validates a molecular dynamics model system that captures the activated enzyme-substrate (E-S) complex. The *in silico* model indicates that FAD-mutant E-S complexes are less conformationally flexible, suggesting complex stabilization, and this is supported by fluorescence lifetime imaging microscopy in intact cells. A *C. elegans* model system for FAD, developed to test mechanisms of neurodegeneration, reveals that stabilization of E-S complexes alone, without production of Aβ peptide products, is sufficient to cause age-dependent synaptic loss and reduced lifespan.

RESULTS

FAD PSEN1 mutations inhibit processive proteolysis of C99 by γ-secretase

Six FAD mutations in presenilin-1 (PSEN1) were separately installed into a tetracistronic pMLINK construct that encodes all four components of the γ-secretase complex,[12] in a multi-step process starting from monocistronic pMLINK encoding human PSEN1 (Figure S1). Wild-type (WT) and FAD-mutant γ-secretase complexes were expressed in and purified from suspension human embryonic kidney (HEK) 293 cells as previously described.[11] Each purified protease variant (30 nM) was incubated with saturating levels (3 μM) of APP-based recombinant substrate C100-Flag at 37 ^{o}C for 16 h, when the rate of substrate cleavage was still in the linear range. Rates of formation of APP intracellular domain (AICD) coproducts AICD50-99 and AICD49-99 (Figure 1A)—produced through initial endoproteolytic (ε) cleavage—were quantified in two steps: quantitative western blotting of total Flag-tagged AICD product, using C100-Flag to

establish a standard curve (Figure 1B), and matrix-assisted laser desorption/ionization-time of flight mass spectrometry (MALDI-TOF MS) to determine the ratio of the two specific AICD products (Figure 1C). All six FAD-mutant enzymes skewed ε cleavage (Figure 1C) toward AICD49-99 and therefore toward the Aβ48→Aβ42 pathway, as previously reported for PSEN1 FAD mutations.[13] All six mutant proteases were also deficient in ε cleavage, with lower rates of production of total AICD, AICD50-99 and AICD49-99 than was seen with WT γ-secretase (Figure 1B,D), which is consistent with previous reports of reduced ε proteolysis with PSEN1 FAD mutations.[14-16] FAD-mutants P117L, G384A and L286V produced ~30-50% less AICD, while I143T, L166P and L435F were >90% deficient in ε proteolysis. Quantification of AICD49-99 and AICD50-99 (Figure 1D) provided indirect quantification of the production of respective ε cleavage coproducts Aβ48 and Aβ49, data that was used below to determine efficiencies of subsequent carboxypeptidase trimming steps.

To quantify the production of each small peptide coproduct of processive carboxypeptidase cleavage by WT and FAD-mutant γ-secretase complexes, APP-based recombinant substrate C100-Flag was expressed in and purified from *E. coli* under conditions that would provide either "light" ($^{12}C/^{14}N$) or "heavy" ($^{13}C/^{15}N$) isotopic labeling (Figure S2). "Light" substrate was incubated with WT γ-secretase, while in parallel "heavy" substrate was incubated with FAD-mutant proteases (Figure 1E). This allowed subsequent mixing of equal volumes of WT and FAD-mutant enzyme reaction mixtures, with detection and direct comparison of tri- and tetra-peptide proteolytic coproducts from the respective reactions through liquid chromatography coupled with tandem mass spectrometry (LC-MS/MS).[10,11] The three most abundant fragment ions of these small peptides were quantified, first using purified synthetic peptides to establish standard curves and then for the mixed 1:1 enzyme reactions with "light" and "heavy" substrates. Separately incubating light and heavy C100Flag substrate with WT γ-secretase, followed by mixing the two samples before LC-MS/MS analysis validated the method, giving equal levels of light and heavy tri- and tetrapeptide coproducts (Figure S3). WT γ-secretase also

produced consistent levels of each peptide in the LC-MS/MS runs when mixed with the different FAD-mutant enzyme reactions (Figure 1F), providing internal standardization to measure the effect of FAD mutation.

Due to the reduced ε proteolytic activity seen with all six mutant protease complexes, formation of each small peptide coproduct was also lower than that produced from the WT enzyme (Figure 1F). Together with the quantification of AICD coproducts, quantification of these small peptides provided the degree of degradation and production of each Aβ product and therefore the percent efficiency of each carboxypeptidase trimming step for WT versus FAD-mutant enzyme (Figure 1G). Five of the six FAD-mutant γ-secretase complexes (with L286V the exception) were deficient in Aβ48→Aβ45 trimming. Reduced Aβ49→Aβ46 trimming was seen with the P117L mutation, while Aβ46→Aβ43 trimming was strongly reduced with I143T, L166P and L435F mutations, and Aβ43→Aβ40 was reduced with P117L, G384A and L286V mutations. The degree of degradation and production for each Aβ peptide also allowed determination of the levels of each Aβ peptide from the enzyme reactions (Table S1). As an additional cross-check of the LC-MS/MS method, the level of detected total AICD was found to be virtually identical with the sum of all calculated Aβ peptide levels produced from each enzyme reaction. Moreover, levels of AICD49-99 and AICD50-99 equaled the sum of Aβ peptides produced from their respective pathways (Table S2). We have reported similar equimolar production of Aβ and AICD from the processing of 14 FAD-mutant APP substrates by WT γ-secretase.[11] These results show that all six FAD PSEN1 mutations led to reduction in early proteolytic processing steps on APP substrate by γ-secretase (ε cleavage, Aβ49→Aβ46, and/or Aβ48→Aβ45 trimming), similar to results with 14 FAD mutations in APP substrate. Specific ELISAs also showed that while all six PSEN1 FAD mutations produce much less Aβ40 and Aβ42 compared to that produced from WT γ-secretase, Aβ40 is consistently reduced more than is Aβ42, thereby increasing the Aβ42/Aβ40 ratio (Figure S4).

Structure of the γ-secretase E-S complex at the transition state

Because FAD mutations alter proteolytic processing of the APP TMD by γ-secretase, we sought a structural dynamic understanding of how the enzyme carries out intramembrane proteolysis. Toward this end, we designed and synthesized a series of full TMD substrate-based peptidomimetics as probes to trap the γ-secretase complex at or near the transition state for structure elucidation by cryo-electron microscopy (cryo-EM).[17,18] These TMD substrate mimetics were composed of a hydroxyethylurea-based transition-state analog,[19] which targets the aspartyl protease active site of γ-secretase on PSEN1, linked to an APP TMD-based peptide containing helix-inducing α-aminoisobutyric acid (Aib) residues,[20] which targets a proximal substrate-binding exosite (Figure 2A).[21] Both peptidomimetic components on their own are moderately potent inhibitors of γ-secretase (50% inhibitory concentrations, or IC_{50}s, in the range of 40-60 nM toward 1 nM enzyme). However, linking them through short 9- or 10-atom spacers resulted in inhibitory potencies approaching stoichiometric levels (IC_{50} of 0.5 nM with 1 nM enzyme).[17,18] Several of these TMD mimetic inhibitors were selected for study with γ-secretase by cryo-EM, and one of these compounds (**SB-250** in Figure 2A), with a triglycine linker, provided an atomic-resolution (2.6 Å) structure (Figures 2B-D, Figure S5, Table S3)

The structure of TMD mimetic **SB-250** bound to γ-secretase (this study) is remarkably similar to that of the enzyme bound to APP substrate[22] (Fig. 2C). In both structures, the N-terminal region of the substrate/mimetic TMD is in a helical conformation and enveloped by PSEN1 TMDs, while the C-terminal region is in an extended conformation that interacts with the active site. However, the protease structure with bound APP substrate was accessed by disulfide crosslinking this substrate to PSEN1 through cysteine mutations as well as using catalytically inactive protease complex, with one of the two PSEN1 TMD aspartates mutated to alanine.[22] In contrast, mimetic **SB-250** is bound noncovalently to the active γ-secretase complex, allowing coordination of the transition state-mimicking moiety with the two catalytic aspartates (Figure 2D). This coordination, within hydrogen-bonding distance, between the

mimetic hydroxyl group and the two PSEN1 TMD aspartates, is closely similar to what has been observed in x-ray crystal structures of water-soluble aspartyl proteases bound to related transition-state analogues.[23-25] Thus, the new structure of TMD substrate mimetic **SB-250** bound to γ-secretase likely reveals the conformation of the enzyme-substrate (E-S) complex at or near the transition state, poised as it would be during intramembrane proteolysis.

FAD mutations stabilize the γ-secretase E-S complex

In parallel with the development and analysis of structural probe peptidomimetics, we also used an *in silico* molecular dynamics system to understand γ-secretase action and the effects of FAD mutations. We recently reported the development of such models, for ε cleavage and the Aβ49→Aβ46 trimming step using all-atom Gaussian-accelerated molecular dynamics (GaMD) simulations.[26-28] In these simulations, water entered the active site and coordinated between the two aspartates, with positioning for nucleophilic attack of the water oxygen on the carbonyl carbon of the scissile amide bond Leu49-Val50. Meanwhile, the carboxylic acid side chain of the protonated aspartate interacted with the oxygen atom of the scissile amide bond, thereby activating the carbonyl carbon for nucleophilic attack by water. These simulations only bring the system to the point where water is poised to attack the carbon atom of the amide bond and cannot follow the hydrolytic reaction itself. Nevertheless, the conformation of the activated enzyme-substrate complex, poised for peptide bond hydrolysis, is in a low-energy state with respect to those not along the reaction pathway. This low-energy conformation, with the enzyme, water and substrate set up for intramembrane hydrolysis, overlaps remarkably well, particularly in the active site, with the new cryo-EM structure with TMD mimetic **SB-250** (Figure 2E). Thus, the new cryo-EM structure provides important support for the GaMD *in silico* simulations.

Given this structural confirmation, the six PSEN1 FAD mutations analyzed for comprehensive effects on γ-secretase cleavage of APP substrate were then examined for

effects on activating the ε cleavage step using GaMD simulations. Consistent with the biochemical analysis, most of the six PSEN1 FAD mutations visited the active conformation less frequently, if at all.[28] Analysis of GaMD simulations of the FAD-mutant E-S complexes further revealed that all six reduced conformational fluctuations compared with the WT E-S complex, in particular for PSEN1 TM6a and the associated region of APP substrate inserted into the active site (Figure 2F). The reduced conformational flexibility suggests a mechanism by which these mutations decrease ε cleavage, as enzyme catalysis is a dynamic process that requires conformational rearrangements. The reduced flexibility further suggests that the FAD-mutant E-S complexes are more stable: Because the substrate is enveloped by PSEN1 TMDs, dissociation of substrate from the enzyme should be slower (i.e., the E-S complex is kinetically stabilized). Additional GaMD simulations were performed for the Aβ49→Aβ46 trimming step. Remarkably, only P117L PSEN1 prevented the Aβ49/γ-secretase complex from visiting the active conformation (Figure 2G), consistent with results from LC-MS/MS analysis of this trimming step (Figure 1G). The complex of P117L PSEN1 γ-secretase with Aβ49 was also found to be the least flexible among the FAD mutations examined compared to the WT enzyme-Aβ49 complex (Figure S6).

To test effects of FAD mutations on the stability of γ-secretase E-S complexes in cultured cells, we conducted fluorescence lifetime imaging microscopy (FLIM).[29] WT or FAD-mutant PSEN1 was exogenously expressed together with C99 in HEK293 cells in which endogenous PSEN1 and PSEN2 were knocked out through CRISPR/Cas9 gene editing.[30] The C99 construct contains human APP C99 with the N-terminal signal peptide sequence for membrane insertion and secretory pathway destination and a C-terminal near-infrared fluorescence protein: miRFP720 (C99-720). After fixing and permeabilization, primary antibodies were added that interact with the N-terminal region of C99/Aβ (mouse antibody 6E10) and to an epitope on γ-secretase component nicastrin that is proximal to the N-terminus of bound APP substrate in cryoEM structures (rabbit antibody NBP2-57365). Secondary antibodies conjugated to

fluorophore were then added: anti-mouse IgG antibody conjugated to Alexa Fluor™ 488 and anti-rabbit IgG antibody conjugated to Cy3 (Figure 3A). Although the 6E10 antibody reacts with both C99 and Aβ, dividing the 6E10-Alexa488 emission by that of C99-720 allows detection of cell compartment(s) with lower or higher 6E10 Alexa488/C99-720 ratios as sites where C99 or intracellular Aβ, respectively, are enriched (Figure 3A).[31,32] Selected cells (n = 7-10) were analyzed by FLIM, with the C99 or Aβ-rich regions of interest (ROIs; 136-141) quantified for each sample for average fluorescence lifetime of Alexa Fluor™ 488 (Figure 3B). For each PSEN1 FAD-mutant sample, fluorescence lifetime was significantly reduced compared to that seen with WT PSEN1, both in the C99 and Aβ-rich areas, indicating that more C99/Aβ is proximal (i.e., bound) to FAD-mutant γ-secretase (Figure 3C). Similar results were seen upon testing effects on FLIM using four FAD mutations located in the C99 TMD (Figure 3D). Use of the acceptor antibody with an epitope on the other side of the protease complex (i.e., distal to the N-terminus of bound C99/Aβ) did not lead to any reduction in fluorescence lifetime (Figure S7). These results support stabilization of E-S complexes by FAD mutations, as suggested by the GaMD simulations. However, while the simulations support kinetic stabilization, the FLIM findings in whole cells suggest thermodynamic stability as well, as they presumably capture steady-state conditions.

Stabilized E-S complexes trigger synaptic loss in *C. elegans*

To develop a convenient *in vivo* system to probe pathogenic mechanisms in FAD, we generated transgenic *C. elegans* lines that coexpress C99 and human PSEN1, with and without FAD mutations, under control of the pan-neuronal *rgef-1* promoter (Figure 4A). Parental line *juIs1* expresses synaptobrevin fused to GFP under control of the *unc-25* promoter, enabling visualization of GABAergic synaptic puncta along the dorsal and ventral nerve cords (Figure 4A). Expression of C99 with the APP signal sequence allows membrane insertion, while expression of human PSEN1 leads to replacement of *C. elegans* orthologues sel-12 and hop-1

in endogenous γ-secretase complexes. Human PSEN1 can fully rescue *SEL-12* mutant phenotypes.[33,34] Thus, C99 and functional PSEN1/γ-secretase complexes should be reconstituted into neuronal membranes of the roundworm for intramembrane proteolysis, allowing the testing of effects of FAD mutations. Coexpression of WT C99 and WT PSEN1 led to *C. elegans* lines with lifespans and numbers of synaptic puncta indistinguishable from those of the parental line. In contrast, coexpression of I45F FAD-mutant C99 (Aβ numbering; Iberian APP mutation[35]) and WT PSEN1 gave transgenic lines with substantially reduced lifespans and age-dependent loss of synaptic puncta beginning on day 3-4 of adulthood (Figure 4B-D, Tables S5-S6). These effects required coexpression of WT PSEN1, as monogenic lines expressing only I45F C99 displayed normal or near-normal lifespans and numbers of synaptic puncta. Thus, the neurodegenerative phenotype is due to the interaction of I45F C99 with WT PSEN1, with the latter likely incorporated as the catalytic component of the γ-secretase complex.

The I45F FAD APP mutation leads to a ~15- to 30-fold increase in the Aβ42/Aβ40 ratio.[11,36,37] This is due to near-complete block of the Aβ46→Aβ43 proteolytic step,[11] because a phenylalanine residue in the P2' position of substrate (i.e., two residues C-terminal to the cleavage site) is highly disfavored.[37] To address whether the synaptotoxic effects of I45F C99 are attributable to Aβ42, we installed an additional V44F mutation, to block Aβ45→Aβ42 proteolysis. *In vitro* γ-secretase assays with LC-MS/MS analysis of small peptide coproducts confirmed that the V44F/I45F double mutation completed blocked both Aβ45→Aβ42 and Aβ46→Aβ43 trimming steps (Figure 5A-C). Moreover, generation of HEK293 cells stably expressing WT, I45F and V44F/I45F C99 revealed that both mutant forms of C99 comigrate with γ-secretase by native PAGE (Figure 5D-F), providing additional evidence for stalled E-S complexes in cells. V44F/I45F C99 generates essentially no Aβ42 (ref. 38; Figure 5B,D); nevertheless, coexpression of this double mutant with WT PSEN1 in *C. elegans* did not rescue the phenotype seen with I45F C99 + WT PSEN1 (Figure 4E-G, Tables S5-S6). Indeed, synaptic loss began even earlier, on day 2 of adulthood. A less severe phenotype was seen with the

monogenic V44F/I45F C99 lines, without exogenous WT PSEN1 expression, possibly due to dysfunctional interaction of this double mutant with endogenous worm γ-secretase complexes. Nevertheless, the complete lack of any rescuing effect of V44F/I45F C99 in the presence of WT PSEN1 indicates that the neurodegenerative phenotype observed is independent of Aβ42.

To test whether the neurodegenerative phenotype is dependent on any form of Aβ, we coexpressed V50F/M51F C99 and WT PSEN1. This double mutation essentially blocks ε cleavage and Aβ production, yet V50F/M51F C99 can bind to γ-secretase and compete with other substrates (i.e., it forms stabilized E-S complexes with little or no processing to Aβ peptides).[37] Coexpression with WT PSEN1 resulted in lines with similar reduced lifespan and number of synaptic puncta as seen with I45F and V44F/I45F C99 (Figure 6A-C, Tables S5-S6). These findings suggest that stalled C99/γ-secretase E-S complexes can cause neurodegeneration in the absence of Aβ production. Intriguingly, while synaptic puncta were reduced quite early—as soon as Day 1 of adulthood—in the V50F/M51F C99 + WT PSEN1 lines, nerve cord synapses apparently regenerated by Day 7-9 to levels seen in the WT C99 + WT PSEN1 lines, suggesting compensatory mechanisms to counter synapse loss. We then tested the effects of PSEN1 FAD mutant L166P, which leads to >90% reduction in ε cleavage of C99 (Figure 1B and ref. 39). Neuronal expression of L166P PSEN1 resulted in reduced lifespan with or without coexpression of WT C99 (Figure 6D, Tables S5-S6). Age-dependent loss of synaptic puncta was also seen in the L166P + WT C99 lines (Figure 6E,F); unfortunately, this analysis was not possible with L166P monogenic lines, due to their over-sensitivity (death) upon exposure to the anaesthetizing agent. We note, however, that in all the other *C. elegans* transgenic lines examined here, synaptic loss always accompanied reduced lifespan. Thus, while FAD-mutant I45F C99 required coexpression of WT PSEN1 for a neurodegenerative phenotype, it is likely that FAD-mutant L166P PSEN1 does not require WT C99. These results suggest that stalled γ-secretase bound to other substrates besides C99 can trigger synaptic loss.

DISCUSSION

Difficulties in elucidating the pathogenic trigger(s) of Alzheimer's disease and discovering effective therapeutics suggests that entities and processes beyond Aβ may be primarily responsible for initiating the cascade of events leading to neurodegeneration and dementia.[40,41] Focusing on FAD should simplify identification of pathogenic mechanisms, as these rare variants of Alzheimer's disease are caused by dominant missense mutations in the substrate and enzyme that produce Aβ. In the present study, full analysis of effects of FAD mutations on all the proteolytic steps in γ-secretase processing of C99 revealed that early events (ε cleavage and/or the first and second trimming steps) are commonly deficient. Elucidation of the structure of γ-secretase bound to a full TMD substrate-based probe provided a snapshot of the enzyme poised at or near the transition state of intramembrane proteolysis, and this structure matched a molecular dynamics model of the activated enzyme. The development of this *in silico* model allowed study of the effects of FAD mutations on the structural dynamic mechanism of γ-secretase processing of C99 substrate and Aβ49 intermediate, revealing that FAD-mutant enzyme-substrate (E-S) complexes that are proteolytically deficient occupy a smaller volume of conformational space. This reduced flexibility suggested that the mutant E-S complexes are stabilized while they are stalled in their proteolytic activities, and this idea was supported by reduced fluorescence lifetimes of labeled antibody probe combinations targeting E-S complexes. The development of a *C. elegans* model for FAD then provided a convenient *in vivo* system to interrogate pathogenic mechanisms, with results pointing to stalled, stabilized E-S complexes as the trigger of synaptic degeneration. These findings contradict an earlier report from Szaraga *et al.*, which suggested FAD mutations *de*stabilize E-S complexes, particularly those involving $A\beta_n$ intermediates.[42] However, that study did not test E-S complex stability *per se*, measuring instead the temperature sensitivity of enzyme activity. Here we provide a structural dynamic mechanism for stabilized FAD E-S complexes and FLIM results in intact cells to measure WT vs. FAD E-S complex stability.

The evidence presented here does not exclude roles for Aβ42 and its aggregated forms in FAD pathogenesis. The dysfunctional proteolytic processing caused by FAD mutations typically—but not always[43]—increases Aβ42/Aβ40, primarily through decreased Aβ40 production, thereby increasing the propensity of Aβ42 to aggregation. Such aggregation can lead to activation of glial cells and neuroinflammation that can aggravate the pathogenic process.[44] Moreover, recently reported human trial results showed that an anti-Aβ antibody, lecanemab (Leqembi), cleared Aβ plaques from the brain and modestly slowed the rate of cognitive decline in Alzheimer's disease.[6] The modest effect on cognitive decline, however, suggests Aβ may not be a primary disease driver. We show here that the stalled process—not the products—of γ-secretase proteolysis of substrates can trigger age-dependent synaptic loss and reduce lifespan in *C. elegans*. In FAD, this stalled process can result from missense mutations in either substrate (APP) or enzyme (presenilin)(Figure 7). Among the >100 identified substrates for γ-secretase, FAD mutations are only found in APP, and this may be due to its high expression in the brain[45] along with its constitutive processing by β-secretase to C99.[46] Mutation of other substrates could lead to stalled E-S complexes, but perhaps not to a high enough level to trigger neurodegeneration. Interestingly, FAD mutations in PSEN1 lead to synaptic degeneration even in the absence of C99 co-expression in our *C. elegans* model. We suggest that endogenous substrates bind to this mutant γ-secretase to form stable E-S complexes. The level of such stalled complexes may be high enough to trigger neurodegeneration, because all or most of these endogenous substrates can become part of stalled complexes. No single substrate on its own though would be sufficient.

While our findings implicate stalled E-S complexes as triggers of FAD pathogenesis, they do not address whether stalled complexes do so through reduced proteolysis of critical γ-secretase substrates (in accord with the Presenilin Hypothesis[47]) or through a gain of toxic function of the stalled complexes *per se*. However, dominant mutations in PSEN1 that lead to loss of function through nonsense-mediated decay are associated with dominantly inherited skin disease and

not neurodegeneration,[48] suggesting stalled E-S complexes as such may trigger neurodegeneration through a gain of toxic function. Interestingly, stalled ribosomes provide a precedent for slowed or stuck processive E-S complexes per se triggering gain of function (in this case, specific cellular stress responses).[49] The question of gain versus loss of function mechanisms of synaptic degeneration will be important for future investigations, along with determining the downstream pathways and networks altered by stalled γ-secretase/substrate complexes. Regarding possible relevance of these findings to sporadic late-onset Alzheimer's disease, we speculate that stalled γ-secretase bound up with substrate, perhaps as a consequence of altered membrane composition and properties (e.g., thickness, fluidity) in the aging brain,[50] may trigger this most common form of the disease (Figure 7). Regardless, a key role of stabilized γ-secretase E-S complexes in FAD pathogenesis has implications for drug discovery for this rare genetic form of the disease, suggesting that the search for stimulators of the stalled complexes, to correct the dysfunctional proteolysis, would be worthwhile.

LIMITATIONS OF THE STUDY

While a comprehensive and quantitative analysis of the effects of FAD mutations on all proteolytic events of γ-secretase processing of C99 was conducted, these were conducted using purified enzyme and substrate using a detergent-solubilized system. Effects of these mutations on γ-secretase processing of C99 in cell membranes may differ. The GaMD simulations lead to an E-S complex with water poised for nucleophilic attack on the amide bond. This activated state of the enzyme resembles the conformation of the enzyme bound to a full TMD substrate analog containing a transition-state mimetic, and the GaMD simulation results with FAD mutations are mostly consistent with biochemical findings. However, no experiments were conducted to test if FAD PSEN1 mutations actually reduce conformational flexibility of E-S complexes. The FLIM experiments in whole cells support stabilization of the E-S complexes by FAD mutations, as suggested by the simulations; however, experiments with purified enzyme

and substrate would provide more direct testing of E-S complex stabilization. For the *C. elegans* model system, exogenous expression in neurons may lead to artifacts. Gene editing of an endogenous worm presenilin (e.g., SEL-12) to knock in FAD mutations would test more physiological expression conditions.

SUPPLEMENTAL INFORMATION

Supplemental information can be found online at…

ACKNOWLEDGMENTS

We thank L. Liu (Harvard Medical School/Brigham and Women's Hospital) for HEK293 cells with PSEN1/2 doubly knocked out through genome editing, P. Arafi (U. Kansas undergraduate researcher) for rendering Figure 7, E. Lundquist (U. Kansas) for access to injection apparatus for transgene insertion into *C. elegans*, and E. Rosa-Molinar and N. Martinez-Rivera for assisting with microscopy at the Microscopy and Analytical Imaging Research Resource Core Laboratory at U. Kansas. This work was supported by grants GM122894, AG66986 and AG79569 from the U.S. National Institutes of Health and a Pilot Project Grant from the University of Kansas Alzheimer Disease Research Center via NIH grant P30 AG072973 (M.S.W.); the National Natural Science Foundation of China (Project 81920108015), the National Key R&D Program (2020YFA0509300) from the Ministry of Science and Technology of China, and the Key R&D Program of Zhejiang Province (2020C04001), Frontier Research Center for Biological Structure, and Start-up funds from Westlake University (Y.S.); and grant 2121063 from the U.S. National Science Foundation (Y.M). This work used supercomputing resources with allocation award TG-MCB180049 through ACCESS, project M2874 through NERSC, the BigJay (NSF award MRI-2117449) and Research Computing Clusters at the University of Kansas.

AUTHOR CONTRIBUTIONS

Conceived and designed experiments: S.D., R.Z., V.N., M.M., H.D., A.N., J.T.D., Y.M., B.D.A., Y.S., M.S.W. Performed experiments: S.D., R.Z., V.N., M.M., H.D., C.O., A.S., A.N. Materials preparation: S.B. Analysis of data: S.D., R.Z., V.N., M.M., H.D., A.N., C.O., J.T.D., A.S., Y.M., B.D.A., Y.S., M.S.W. Contributed to the writing and editing of the manuscript: S.D., R.Z., V.N., M.M., H.D., J.T.D., Y.M., B.D.A., Y.S., M.S.W.

DECLARATION OF INTERESTS

The authors have no competing interests to declare.

FIGURE LEGENDS

Figure 1. FAD PSEN1 mutations inhibit processive proteolysis of C99 by γ-secretase.

(A) Schematic of proteolytic processing of APP substrate by γ-secretase. (B) Quantitative western blotting of total AICD, using purified substrate C100Flag to generate a standard curve for densitometry. (C) MALDI-TOF analysis shows ratios of peak heights of AICD49-99/AICD50-99 produced by γ-secretase with WT versus six FAD mutants of PSEN1. (D) Quantification of AICD49-99 and AICD50-99 production, corresponding to Aβ48 and Aβ49 production, respectively. (E) Schematic of light- vs. heavy-isotope labeling of APP substrate for LC-MS/MS analysis of effects of PSEN1 FAD mutations on carboxypeptidase trimming steps. (F) Bar graphs of small peptide coproduct for each trimming step. Blue graphs: first, second and third trimming step for the Aβ49→Aβ40 pathway. Red graphs: trimming steps for the Aβ48→Aβ38 pathway. Dark and light bars: coproduct formation from WT and FAD-mutant γ-secretase, respectively. (G) Bar graph of percent cleavage efficiencies of each trimming step relative to WT enzyme. Where the level of precursor Aβ peptide for a given trimming step is zero, the efficiency

of this cleavage event could not be determined (nd). In all graphs, n=3, unpaired two-tailed T-test compared FAD mutant to WT, *p≤ 0.05, **p≤ 0.01, ***p≤ 0.001.)

Figure 2. Structure of the γ-secretase E-S complex at the transition state and effects of FAD PSEN1 mutations. (A) Schematic of substrate-based structural probe design and specific probe **SB-250**. (B) The overall cryo-EM structure of **SB-250** bound to WT γ-secretase complex. **SB-250** is shown in sticks. (C) The conformation of active PSEN1 (cyan) in complex with **SB-250** (red) shows high similarity with catalytically inactive PSEN1 (yellow) covalently crosslinked to APP-C83 (marine). Superimposition of these two PSEN1 molecules reveals an r.m.s.d. (root-mean-square distance) of 0.428 Å over 250 Cα atoms. (D) The structural probe traps active γ-secretase at the transition-state of intramembrane proteolysis. Note the rotation about the Cα-Cβ bond of catalytic residue D257 in **SB-250**-bound active γ-secretase compared to APP-C83-bound inactive enzyme (see curved arrow), positioning the aspartyl carboxylate for coordination with the transition-state-mimicking hydroxyl group of **SB-250**. (E) Overlap of the cryo-EM structure of substrate mimetic probe bound to γ-secretase with the activated E-S complex from GaMD simulations reveals close similarity of the alignment and orientation of the active site aspartates, with respect to each other as well as with substrate/mimetic. Catalytic D257 and D385 are green for cryoEM structure and yellow for GaMD simulation. (F) GaMD simulations of γ-secretase bound to C99 substrate show overall reduced flexibility with FAD PSEN1 mutations, implying complex stabilization. Root-mean-square fluctuations (RMSFs) of PSEN1 and C99 substrate within E-S complexes were calculated by averaging the RMSFs from individual MD simulations of each γ-secretase system. Changes in RMSFs (ΔRMSF) from WT to FAD-mutant PSEN1 were calculated by subtracting RMSFs of the WT E-S complexes from those with FAD-mutant PSEN1. (G) Free energy profiles of WT and six FAD PSEN1 mutations from GaMD simulations of the Aβ49→Aβ46 trimming step.

Figure 3. FAD PSEN1 mutations stabilize γ-secretase E-S complexes. (A) Design of fluorescence lifetime imaging microscopy (FLIM) experiments. (B) Microscopic imaging with pseudo color analysis to identify C99 or Aβ intermediates-rich subcellular areas (regions of interest, ROIs; circles), followed by FLIM in HEK293 cells. (C) Quantification of FLIM results reveal FAD mutations in PSEN1 and (D) C99 increase stabilization of enzyme-C99 (left panels) or enzyme-Aβ intermediate complexes (right panels) in intact cells. For all graphs, n = 136-141 ROIs from 7-10 cells, one-way ANOVA and the Tukey's multiple comparisons test, n.s., p>0.05* p<0.05, ** p<0.01. *** p<0.001, ****p<0.0001.

Figure 4. Aβ42-independent synaptic loss in *C. elegans* model of FAD. (A) Design of *C. elegans* transgenic model and visualization of synaptic puncta in the parental *juIs1* line. Transgenic lines were obtained by microinjection of human APP C99 and/or human PSEN1 (driven by pan-neuronal *rgef-1* promoter) into the parental line *juIs1. rol-6* (dominant roller) was used as the coinjection marker to select for transformants. *Right*: a representative confocal image showing a series of synaptic puncta marked by GFP-tagged synaptobrevin along the dorsal nerve cord of *juIs1*. (B) Life span of double transgenic lines C99 + PSEN1 and C99 I45F + PSEN1 and monogenic line C99 I45F. Kaplan-Meier curves of n animals show the fraction of animals alive at different days. (C) Quantification of the dorsal and ventral synaptic puncta in the transgenic lines. Average number of synaptic puncta per 100 μm in n transgenic worms for each day is shown in the vertical box plots. Horizontal lines at the top and bottom of each box represent the maximum and minimum values, respectively. Upper and lower ends of a box mark quartiles Q1 and Q3 values, respectively. The horizontal line inside the box shows the median value and marks Q2). Two-way ANOVA for all possible pairs using Tukey's post hoc test, *p≤ 0.05, **p≤ 0.01, ***p≤ 0.001, ****p< 0.0001. Statistical differences shown only for earliest day significance was seen compared to Day 1 in a given line. (D) 100 μm sections of representative confocal microscopic images dorsal (left) and ventral (right) nerve cords of transgenic animals.

's' denotes average number of synaptic puncta per 100 μm from n animals. (E) Life span of double transgenic line C99 V44F/I45F + PSEN1 and monogenic line C99 V44F/I45F compared with C99 + PSEN1 and C99 I45F + PSEN1 lines. (F) Quantification of dorsal and ventral synaptic puncta in these transgenic lines. Two-way ANOVA for all possible pairs using Tukey's post hoc test, *p≤ 0.05, **p≤ 0.01, ***p≤ 0.001, ****p< 0.0001. Statistical differences shown only for earliest day significance was seen compared to Day 1 in a given line. (G) 100 μm sections of representative confocal microscopic images of dorsal and ventral synaptic puncta in these transgenic lines. All experiments shown in Fig. 4 were repeated with independent transgenic lines, giving similar results.

Figure 5. V44F/I45F double mutation of APP substrate blocks Aβ46→Aβ43 and Aβ45→Aβ42 cleavage steps by γ-secretase and stabilizes E-S complexes. (A) Transmembrane domain sequence alignment of WT versus V44F/I45F C99. (B) Concentration of tri- or tetra-peptides detected by LC-MS/MS analysis from WT C100-FLAG and V44F/I45F C100-FLAG. Cleavage events along the Aβ40 pathway are represented by ITL→VIV→IAT (blue) and cleavage events along the Aβ42 pathway are represented by VIT→TVI→VVIA (red). Note that cleavage steps from Aβ46→Aβ43 and Aβ45→Aβ42 for the V44F/I45F mutation produce tripeptides FFV and TFF, respectively. Notation "nd" indicates tri- or tetra-peptides unable to be detected by LC-MS/MS. 30 nM of enzyme and 5 μM of substrate were incubated at 37 ^{o}C for 16 h for both trials. The average and range of both trials is represented in the graph. (C) MALDI-TOF mass spectrometric analysis of AICD 50-99 and AICD 49-99 produced by γ-secretase with WT versus V44F/I45F C100-FLAG. Note the V44F/I45F double mutation leads to substantially reduced AICD50-99 production. (D) Secreted Aβ40 and Aβ42 levels in the culture media of HEK-293 cells stably expressing C99 and its mutants I45F and V44F/I45F were measured by specific ELISAs. Aβ42/Aβ40 ratios are also indicated. "NT" indicates the non-

transfected (NT) control. Data are the mean ± S.E. from three independent experiments. (E) Cellular C99 levels in HEK-293 cells stably expressing C99 and its mutants were examined by Western blotting using monoclonal antibody 6E10. (F) 10 μg of protein from the various HEK-293 cell lysates were subjected to BN-PAGE (1% digitonin) or SDS-PAGE and analyzed by Western blotting using antibodies specific for C99/Aβ, PS1-NTF and GAPDH. Data are representative of three independent experiments.

Figure 6. Stabilized E-S complexes trigger synaptic loss in *C. elegans*. (A) Life span analysis of double transgenic line C99 V50F/M51F + PSEN1 compared with C99 + PSEN1, C99 I45F + PSEN1 and C99 V44F/I45F + PSEN1 lines. (B) Quantification of dorsal and ventral synaptic puncta in these transgenic lines. Two-way ANOVA for all possible pairs using Tukey's post hoc test, *p≤ 0.05, **p≤ 0.01, ***p≤ 0.001, ****p< 0.0001. Statistical differences shown only for earliest day significance was seen between a given line versus C99 + PSEN1. (C) 100 μm sections of representative confocal microscopic images of dorsal and ventral synaptic puncta in these transgenic lines. The same data used in Fig. 4 for C99 + PSEN1, C99 I45F + PSEN1 and C99 V44F/I45F + PSEN1 were reproduced in panels B-D for direct comparison with C99 V50F/M51F + PSEN1. (D) Life span analysis of double transgenic line C99 + PSEN1 L166P and single transgenic line PS1 L166P compared with C99 + PSEN1. (E) Quantification of dorsal and ventral synapses in double transgenic lines C99 + PSEN1 and C99 + PSEN1 L166P. *Note*: PS-1 L166P monogenic lines were sensitive to the anesthetic agent, phenoxy propanol, leading to dying on agarose pads during sample preparation for imaging. Thus, confocal imaging of these animals was not possible. Two-way ANOVA for all possible pairs using Tukey's post hoc test, *p≤ 0.05, **p≤ 0.01, ***p≤ 0.001, ****p< 0.0001. Statistical differences shown only for days significance was seen within a given line. (F) 100 μm sections of representative fluorescence microscopic images of dorsal and ventral synaptic puncta in these transgenic lines. The same

data used in Fig. 4 for C99 + PSEN1 were reproduced in panels D-F for direct comparison with C99 + PSEN1 L166P and PSEN1 L166P (lifespan) or with only C99 + PSEN1 L166P (synaptic puncta). All experiments shown in Fig. 6 were repeated with independent transgenic lines, giving similar results.

Figure 7. Model for how FAD mutations trigger pathogenesis and possible implications for sporadic Alzheimer's disease. In healthy neurons, the γ-secretase complex can effectively process C99 and the enzyme's many other membrane-bound substrates. FAD mutations in APP result in stalled γ-secretase complexes bound to C99 substrate or Aβ intermediate. FAD mutations in presenilin result in stalled interaction between γ-secretase and its substrates (not restricted to C99). In sporadic late-onset AD, in the absence of mutations in APP or presenilins, other factors, such as altered membrane fluidity or thickness, may stabilize E-S complexes, thereby triggering synaptic degeneration.

STAR METHODS

RESOURCE AVAILABILITY

Lead contact

Further information and requests for resources and reagents should be directed to and will be fulfilled by the Lead Contact, Michael S. Wolfe (mswolfe@ku.edu).

Materials availability

Plasmid constructs, stably tranfected HEK293 cell lines, and transgenic *C. elegans* lines will be made available upon request. However, quantities of structural probe compound SB-250 are limited; availability will depend on the amount requested and the number of such requests.

Data and code availability

CryoEM map of the structure of γ-secretase bound to probe SB-250 has been deposited in the Electron Microscopy Data Bank (EMDB) under the ID code EMD-36948. Atomic model for the structure of γ-secretase bound to probe SB-250 has been deposited in the Protein Database (PDB) under the ID code 8K8E.

EXPERIMENTAL MODEL AND SUBJECT DETAILS

Cell lines used in this study

HEK293F, a human embryonic kidney cell line purchased from Invitrogen, was used for protein production of γ-secretase complexes. HEK293, an adherent version of this same cell line purchased from ATCC, was used to generate stably transfected lines expressing APP C99 and mutants thereof. HEK293 with PSEN1/2 double knockout by CRISPR (ref. 30), a gift of Dr. Lei Liu (Brigham and Women's Hospital, Harvard Medical School, Boston, MA), was used for transfection and fluorescence lifetime imaging microscopy.

Cell culture conditions

HEK 293F cells were grown in unsupplemented Freestyle 293 media (ThermoFisher, 12338018). Transient transfection was performed when the cell density reached 2 x 10^6 cells/mL. The cells were maintained at 37 ^oC with 130 rpm/min under 5% CO_2. HEK293 cells (nontransfected control line, stably transfected C99 lines, and the PSEN1/2 double knockout HEK293 line) were cultured in Dulbecco's modified Eagle's medium (DMEM; GIBCO, USA) supplemented with 10% fetal bovine serum (FBS; GIBCO, USA) at 37°C and 5% CO_2.

Bacterial strains and culture

E. coli DH5α (Invitrogen) was used for molecular cloning and plasmid preparation and were grown in LB media at 37 ^{o}C with continuous shaking. *E. coli* BL21 (DE3), used for transduction and expression of γ-secretase substrate C100Flag, was grown in LB media at 37 ^{o}C with continuous shaking to OD600 0.6, whereupon expression was induced with 0.5 mM IPTG.

***C. elegans* strains and maintenance**

Animals were maintained on nematode growth medium (NGM) plates and fed *E. coli* OP50. Transgenic lines were obtained by injecting human C99 and/or PSEN1 constructs with co-injection marker *rol-6* into gonads of *juIs1* [*Punc-25*::SNB-1::GFP]. F1 and F2 generations were selected based on the roller phenotype of the co-injection marker.

METHOD DETAILS

^{15}N, ^{13}C labelled C100-FLAG expression and purification

E. coli BL21 cells transformed with C100-FLAG construct in pET22b vector[51] were grown with shaking in minimal media with 20% ^{13}C glucose (Cambridge Isotope Laboratories and $^{15}NH_4Cl$ (Cambridge Isotope Laboratories) at 37 ^{0}C until OD_{600} reached 0.8. The minimal media composition is listed in Fig S2. Cells were induced with 0.5 mM IPTG and grown for 3 h. Cells were harvested by centrifugation, resuspended in lysis buffer composed of 25 mM Tris pH 8 and 1% Triton X-100, and lysed passing through a French press three times. Cleared lysate was incubated with anti-FLAG M2-agarose beads (Sigma-Aldrich) for 16 h with shaking at 4 ^{o}C. The beads were washed 3 times with lysis buffer, and C100-FLAG protein was eluted with buffer composed of 100 mM glycine at pH 2.7 and 0.25% NP-40, followed by neutralization with pH 8

Tris buffer and storage at -80 ^{0}C. The identity and purity of C100-FLAG was analyzed by SDS/PAGE with Coomassie staining and MALDI-TOF mass spectrometry.

FAD-mutant γ-secretase constructs

Four monocistonic pMLINK vectors, pMLINK-PSEN1, pMLINK-Aph1 (with C-terminal HA epitope tag), pMLINK-NCT (with C-terminal V5 and 6XHIS epitope tags) and pMLINK-Pen-2 (with N-terminal STREP and FLAG epitope tags), were constructed as previously described.[12] FAD mutations were made in the PSEN1 coding region of pMLINK-PSEN1 by site-directed mutagenesis (QuikChange Lightning Multi-Site Directed Mutagenesis kit, Agilent). Each vector has LINK1 and LINK2 sequences flanking the gene of interest. LINK1 harbors a Pac1 restriction site and LINK2 harbors both PacI and Swa1 restriction sites. Mutated pMLINK-PSEN1 vector was treated with restriction enzyme Pac1 and electrophoresed through 1% agarose gel to separate and purify the FAD-mutant PSEN1 DNA. Similarly, pMLINK-APhH1 was treated with SwaI restriction enzyme to linearize the vector followed by electrophoresis through 1% agarose gel and gel band isolation. The PSEN1 fragment and linearized pMLINK-APhH1 vector were treated with T4 polymerase for 20 min at ambient temperature in the presence of dCTP or dGTP, respectively. The purified T4 polymerase-treated PSEN1 fragment was inserted into purified linearized pMLINK-Aph1 by ligation independent cloning (LIC) to create bicistronic pMLINK-Aph1-PSEN1 vector. Similarly, bicistonic pMLINK-Pen2-Nicastrin was created using the LIC method. Finally, the two bicistronic vectors were used to make the tetracistronic vector (pMLINK-PEN-2-nicastrin-APH-1-PS1) by the LIC method (See Fig. S1 for illustration).

γ-Secretase expression and purification

γ-Secretase was expressed and purified from HEK 293F cells as described previously.[52-54] Briefly, HEK 293F cells were grown in unsupplemented Freestyle 293 media (ThermoFisher, 12338018) until cell density reached 2 x 10^6 cells/mL. For transfection, media was replaced with fresh Freestyle 293 media. 150 mg pMLINK tetracistronic vector and 450 mg polyethylenimines of 25 kDa (PEI) was mixed in 5 mL of Freestyle media followed by incubation for 30 min at ambient temperature. The incubated DNA/PEI mixture was added to the cell culture, which after 24 h was sub-cultured in three flasks and further grown for 36 h before harvesting. Cells were pelleted by centrifugation and resuspended in buffer consisting of 50 mM MES pH 6.0, 150 mM NaCl, 5 mM $CaCl_2$ and 5 mM $MgCl_2$, and lysed by French press. Unbroken cells and debris were pelleted by centrifugation at 3000 x g for 10 minutes. The supernatant was ultracentrifuged at 100,000 x g for 1 h to isolate the membrane pellet. The membrane pellet was washed with 0.1 M sodium bicarbonate pH 11.3 by successive passage through syringes with 18-, 22-, 25- and 27-gauge needles, followed by ultracentrifugation at 100,000 x g for 1 h. The pellet was resuspended in 50 mM HEPES pH 7, 150 mM NaCl and 1% CHAPSO, and incubated in ice for 1 h, followed by ultracentrifugation at 100,000 x g. The supernatant was mixed with anti-FLAG M2-agarose beads (Sigma-Aldrich) and TBS with 0.1% digitonin and incubated for 16 h at 4 ^oC. Beads were washed three times with TBS/0.1% digitonin before eluting the γ-secretase complex with buffer consisting of 0.2 mg/mL FLAG peptide in TBS/ 0.1% digitonin. The eluate was stored at -80 ^0C until further use.

In vitro γ-secretase assay

In vitro γ-secretase assay was performed as described previously.[11] Briefly, 30 nM of WT or FAD mutant γ-secretase was preincubated for 30 min at 37 °C in assay buffer composed of 50 mM HEPES pH 7.0, 150 mM NaCl, and 0.25% 3-[(3-cholamidopropyl) dimethylammonio]-2-

hydroxy-1-propanesulfonate (CHAPSO), 0.1% phosphatidylcholine and 0.025% phosphatidylethanolamine. Reactions were started by adding either the light- or heavy-isotope form of C100-FLAG substrate (3 μM final concentration) and incubating at 37 ^{o}C for 16 h. The reactions were stopped by flash freezing in liquid nitrogen and stored at -20 ^{o}C.

Tri- and tetra peptide products analysis by LC-MS/MS

Small peptides were analyzed using an ESI Quadrupole Time-of-Flight (Q-TOF) mass spectrometer (Q-TOF Premier, Waters) by LC-MS/MS as described previously.[11] The reaction mixture consisting of light C100-FLAG/WT γ-secretase and reaction mixture consisting of heavy C100-Flag/FAD γ-secretase were mixed 1:1 prior to injection onto a C18 analytical chromatography column and eluted with a step gradient of 0.08% aqueous formic acid, acetonitrile, isopropanol, and a 1:1 acetone/dioxane mixture. The three most abundant fragments from collision-induced dissociation were identified by tandem MS for each small peptide. Similarly, various concentrations of the synthetic peptides' standards (>98% purity, New England Peptide) were dissolved in assay buffer and loaded onto a C18 analytical chromatography column for LC-MS/MS analysis. To obtain a peptide chromatographic area, the signals from the 3 most abundant ions were summed using an ion mass width of 0.02 unit. Data were acquired in "V" mode.

Immunoblotting of AICD products

For quantitative immunoblotting of total AICD-Flag products, γ-secretase reaction samples and C100-FLAG standards were run on SDS-PAGE 4-12% Bis-Tris gels and transferred to PVDF membranes. Membranes were blocked with 5% dry milk for 1 h at ambient temperature and treated with anti-Flag M2 antibodies (Sigma-Aldrich) for 16 h at 4 ^{o}C. The blot was then washed

3 times and incubated with anti-mouse secondary antibodies for 1 h at ambient temperature. The membrane was washed and imaged for chemiluminescence, and bands were analyzed by densitometry. A standard curve established from a concentration range of C100-FLAG protein was used to calculate AICD-FLAG product concentration from the enzyme reaction mixtures.

Detection of AICD species by mass spectrometry

AICD-FLAG in the reaction mixture was immunoprecipitated with anti-FLAG M2 beads (Sigma-Aldrich) in 10 mM MES pH 6.5, 10 mM NaCl, 0.05% DDM detergent for 16 hours at 4 ^{o}C. AICD products were eluted from the anti-FLAG beads with acetonitrile:water (1:1) with 0.1% trifluoroacetic acid. The elutes were analyzed on a Bruker Autoflex MALDI-TOF mass spectrometer.

Quantification of Aβ40 and Aβ42 by ELISA

To measure secreted Aβ peptides, conditioned media were collected after 48 h from confluent HEK293 cells (nontransfected control line and those stably transfected with variants of C99). Levels of secreted Aβ40 and Aβ42 in the conditioned media were measured with specific ELISA kits from Invitrogen according to the manufacturer's instructions. All samples were measured in triplicate. Similarly, levels of Aβ40 and Aβ42 derived from *in vitro* cleavage assays with purified γ-secretase complexes and C100Flag substrate were determined.

Cell culture and DNA transfection for C99-expressing HEK293 cells

Human embryonic kidney 293 (HEK293) cells stably expressing human C99, and its mutants were cultured in Dulbecco's modified Eagle's medium (DMEM; GIBCO, USA) at 37°C and 5%

CO_2. All cell lines were grown in this medium supplemented with 10% fetal bovine serum (FBS; GIBCO, USA). HEK293 cells were transfected using Lipofectamine 3000 (Thermo Fisher Scientific, USA) with the cDNA of human C99 with the APP signal sequence inserted into pCMVvector containing a puromycin resistance gene[55] (gift of L. Liu, Brigham and Women's Hospital, Boston). Two different mutant forms of C99 were transfected separately: 1) "C99-F", containing the I45F Iberian FAD mutation; 2) "C99-FF", further containing an artificial V44F mutation that blocks Aβ42 production. After transfection, cells were treated with puromycin (1 mg/ml) to select for cells stably expressing the C99 variants.

Antibodies and Western blot analysis for C99-expressing HEK293 cells

The following antibodies were used: Anti-GAPDH (Cell Signaling Technology, 97166), Anti-PS1-NTF (Bio-Legend, 823401), anti-Aβ 6E10 (Bio-Legend, 803001), Anti-total Aβ (Cell Signaling Technology, 8243). Western blot analysis was performed using standard techniques. Cells were lysed in 1% digitonin and a protease inhibitor mixture, protein levels determined via BCA assay (Thermo Fisher Scientific, USA), and protein-normalized lysates were subjected to SDS-PAGE and transferred to PVDF membranes. Immunoblot analysis was then performed and visualized by the enhanced chemiluminescence method.

Blue native–polyacrylamide gel electrophoresis (BN-PAGE) from C99-expressing HEK cells. Cells were lysed in a native sample buffer (Thermo Fisher Scientific, USA) containing 1% digitonin and a protease inhibitor mixture. After centrifugation at 20,000 X g at 4 °C for 30 min, the supernatant was separated on a 3–12% BisTris gel (ThermoFisher Scientific, USA) according to the instructions of the Novex BisTris gel system (ThermoFisher Scientific, USA).

The transferred blot was incubated in 20 mL of 8% acetic acid for 15 minutes to fix the proteins, rinsed with deionized water and analyzed with Western blotting.

Sample preparation for cryo-EM study

The γ-secretase complex was purified as previously described.[12] The peak fractions from gel filtration were concentrated to ~40 μM to incubate with 1.5 mM of transmembrane substrate mimitic SB-250 (final concentration) for 1 h at 4 °C. Cryo-EM grids were prepared with a Vitrobot (FEI). Aliquots of 4 μL of the SB-250-protein mixture were added to glow-discharged grids (Quantifoil Au R1.2/1.3). The grids were blotted for 3 s and frozen by liquid ethane, and then transferred to liquid nitrogen for storage.

Data collection and processing for cryo-EM analysis

The prepared grids were imaged on an FEI 300 kV Titan Krios electron microscope equipped with GIF Quantum energy filter (slit width 20 eV) and Gatan K3 Summit detector with a nominal magnification of 81,000 × (pixel size 1.0825). 8,324 micrographs were collected in total. MotionCor2 and Gctf were subsequentially used for motion correction and defocus value estimation, respectively. 3,556,137 particles were auto-picked with RELION (version 3.0) and were subjected to two-dimensional (2D) classification. 2, 182, 400 particles were then selected for 50 iterations of global angular search three-dimensional (3D) classification with a class number of 1 and step size of 7.5°. For the last six iterations (No. 45-50) of the global search, the local angular search 3D classification was performed with a class number of four, a step size of 3.75°, and a local search range of 15°. For the last iteration of the local search, particles from the good classes were merged and duplicated particles were removed, yielding 1,561,706 particles. Then we generated multi-reference models from one of the last iterations of local

search 3D classification. The merged particles were applied to multi-reference-based 3D classification. Finally, 349,532 particles from the good classes were auto-refined, resulting in 3.4-Å reconstruction. After mask application, increasing box size and postprocessing, a final reconstruction of 2.6-Å was achieved based on the Fourier shell correlation (FSC) 0.143 criterion.[56] Local resolution estimation was performed using RELION-3.0.[57]

Aβ49→Aβ46 molecular dynamics simulation system setup

Starting from the "Active" WT conformation obtained from a previous study,[58] the amide bond between APP residue L49 and V50 was cleaved to prepare the starting structure. The PS1 FAD mutations, including G384A, I143T, L166P, L286V, L435F, and P117L, were computationally generated using the *Mutation* function of CHARMM-GUI.[59-62] Here, residue D385 in PS1 was protonated and the C-terminal of Aβ49 and N-terminal of AICD50-83 were charged to simulate γ-secretase activation for ζ cleavage of Aβ49 based on previous studies.[58,63] Other chain termini were capped with neutral patches (acetyl and methylamide). The γ-secretase complexes were embedded in POPC membrane lipid bilayers and solvated in 0.15 M NaCl solutions using the CHARMM-GUI webserver.[59-62]

Simulation protocols

Gaussian-accelerated molecular dynamics (GaMD) simulations of WT and PS1 FAD mutant γ-secretase bound by APP-C99 (i.e., to simulate activation for ε cleavage) were obtained from a previous study[58]. The CHARMM36m force field parameter set[64] was used for the protein lipids. The simulation systems were initially energetically minimized for 5000 steps using the steepest-descent algorithm and equilibrated with the constant number, volume, and temperature (NVT) ensemble at 310 K. They were further equilibrated for 375 ps at 310 K with the constant

number, pressure, and temperature (NPT) ensemble. Short conventional molecular dynamics (cMD) simulations were then performed for 10 ns using the NPT ensemble with constant surface tension at 1 atm and 310 K. All-atom Peptide Gaussian accelerated molecular dynamics (Pep-GaMD) implemented in the GPU version of AMBER 20[65,66] was applied to simulate the effects of PS1 FAD mutations on γ-secretase activation for cleavage of Aβ49 to Aβ46. The dual-boost scheme of all-atom Pep-GaMD (igamd = 18) was used in the new simulations of the WT and PS1 FAD mutant γ-secretase bound by the Aβ49 peptide substrate and AICD50-99. In particular, selective boost potential was applied to the essential potential energy of the peptide (Aβ49 and AICD50-99). Another boost potential was applied to the rest of the simulation system. The threshold energy E for adding total boost potential was set to the upper bound, i.e., $E_P = V_{minP} + (V_{maxP} - V_{minP}) / k_{0P}$, whereas the threshold energy E_D for adding dihedral boost potential was set to the lower bound, i.e., $E_D = V_{maxD}$.[66,67] The upper limits of the boost potential standard deviations, σ_{0P} and σ_{0D}, were set to 8.0 kcal/mol and 6.0 kcal/mol, respectively. The PepGaMD simulations involved an initial short cMD of 15 ns to calculate acceleration parameters and equilibration of added boost potentials for 60 ns. Three 600 ns independent production simulations with randomized initial atomic velocities were performed on the γ-secretase complexes.

Simulation analysis

The simulation trajectories were analyzed using VMD[68] and CPPTRAJ.[69] Root-mean-square fluctuations (RMSFs) of PS1 and substrate within the γ-secretase complexes were calculated by averaging the RMSFs calculated from individual PepGaMD simulations of each γ-secretase system. Changes in the RMSFs (ΔRMSF) from the WT to PS1 FAD mutant γ-secretase were calculated by subtracting the RMSFs of the WT from those of PS1 FAD mutant γ-secretase (Fig. 2F and Fig. S6). In GaMD, overall shape of the original potential energy surface is maintained when adding boost potential to enhance conformational sampling of biomolecules. Therefore,

GaMD simulations still sample relevant conformations, from which RMSFs can be reasonably calculated and compared, provided that the added boost potentials are similar between the compared systems, as was the case here (Table S4). The distance between Cγ atoms of catalytic aspartates PS1-D257 and D385 and distance between PS1 residue D385 (atom OD2) and Aβ49 residue V46 (atom O) were calculated. The PyReweighting[70] toolkit was applied for free energy calculations from the D257-D385 and D385-V46 distances for each system (Fig. 2G). A bin size of 1 Å and cutoff 500 frames in each bin was used to calculate the two-dimension (2D) potential mean force (PMF) free energy profiles.

Plasmid DNA for Fluorescence Lifetime Imaging Microscopy Experiments

The C99-720 plasmid, which contains APP signal peptide, human APP C99, FLAG tag, and miRFP720, was sub-cloned from the C99 miRFP720-miRFP670 (C99 720-670) biosensor[71] into pcDNA3.1 (+) empty vector using NheI/EcoRI. Then, mutagenesis was performed to introduce the stop codon after the miRFP720 sequence using primers FW: ATCGGCGTGATGGAAGAGTAAGAATTCTGCAGATATCCA and RV: TGGATATCTGCAGAATTCTTACTCTTCCATCACGCCGAT. The plasmid sequence was verified by the MGH CCIB DNA core.

Immunocytochemistry

PSEN1/2 dKO HEK293 cells[30] co-transfected with C99-720 and WT or FAD-mutant PSEN1 were fixed with 4% paraformaldehyde (PFA) (VWR, Radnor, PA), and permeabilized by 0.1% Triton-X100 (Sigma-Aldrich, St. Louis, MO). The permeabilized cells were then incubated with mouse monoclonal 6E10 (BioLegend, San Diego, CA) and rabbit polyclonal nicastrin antibodies (Novus Biologicals, LLC, Centennial, CO), followed by an Alexa Fluor™ 488 (FRET donor) or

Cy3 (acceptor)-conjugated anti-mouse and rabbit IgG secondary antibodies, respectively (ThermoFisher Scientific). For control experiment in Fig. S7, primary antibody to PSEN1 Loop (EP2000Y; Abcam) was used in place of anti-nicastrin antibody. The slide was covered by a coverslip using Fluoromount-G™ Mounting Medium (ThermoFisher Scientific) and stored at 4 ºC.

Confocal microscopy and fluorescence lifetime imaging microscopy (FLIM)

An Olympus FV3000 Confocal Laser Scanning Microscope (Tokyo, Japan) was used to perform confocal microscopy and FLIM. Lasers at 488 nm, 561 nm, and 640 nm were used to excite an Alexa Fluor™ 488, Cy3, and C99-720, and the emitted fluorescence was detected within 500-530 nm (6E10-Alexa 488), 560-590 nm (nicastrin-Cy3), and 700-800 nm (C99-720) using a 40x/0.95NA objective. Pseudo-colored images corresponding to the ratios of 6E10-Alexa Fluor™ 488 over C99-720 emission were generated in MATLAB (MathWorks, Natick, MA).

In FLIM analysis, a mode-locked Chameleon Ti: Sapphire laser (Coherent Inc., Santa Clara, CA) set at 850 nm was used to excite an Alexa Fluor™ 488 fluorophore (FRET donor), and the emission was collected using the ET525/50m-2p filter (Chroma Technology Corp, Bellows Falls, VT). The donor Alexa Fluor™ 488 lifetime was recorded using a high-speed photomultiplier tube (MCP R3809; Hamamatsu photonics, Hamamatsu City, Japan) and a time-correlated single-photon counting acquisition board (SPC-830; Becker & Hickl GmbH, Berlin, Germany). The acquired FLIM data were analyzed using SPC Image software (Becker & Hickl GmbH). The donor Alexa 488's average lifetime (t1) was first measured in the absence of the acceptor fluorophore (Cy3) (donor only/FLIM negative control). Then, the donor Alexa 488's average lifetime was recorded in the presence of the acceptor Cy3 fluorophore (t2). The proximity between the donor and acceptor (less than 5–10 nm apart) results in energy transfer from the donor to the acceptor (FRET present), yielding characteristic shortening of t2.

C. elegans transgenes

C. elegans was maintained on nematode growth medium (NGM) plates and fed *E. coli* OP50.[72] *juIs1* strain [unc-25p::snb-1::GFP + lin-15(+)] expresses GFP fused to synaptobrevin in presynaptic terminals of GABAergic dorsal and ventral nerve cord neurons.[73] Human APP C99 and PS-1 cDNA were synthesized by GeneArt through ThermoFisher. Human C99 constructs include DNA encoding APP signal peptide (APP_{1-17}: MLPGLALLLLAAWTARA) followed by APP C99. These constructs were designed to include worm introns. All human constructs were cloned in worm expression vector pEVL415 (P*rgef-1*:*htau40::gfp::unc-54* 3′UTR).[74] The vector was linearized, with excision of *htau40:gfp* DNA, by restriction digestion with BamH1 and NgoM4. PCR was performed to amplify the genes of interest from the constructs carrying them using primers that were designed to have ~ 15 bp 5' extensions complementary to the 3' sticky ends of the linearized vector. Cloning was performed by In-Fusion cloning (TakaraBio) following manufacturer's protocol. *C. elegans* carrying extra-chromosomal arrays of transgenic plasmids (human C99APP and/or human PS-1) were generated using pRF4 as a co-injection marker.

Plasmids generated in the study :

1 pEVL545 [*Prgef-1*::signal peptide : human wt C99APP :: *unc-54* 3'UTR]

2 pEVL546 [*Prgef-1*::signal peptide : human C99APP (I45F) :: *unc-5*4 3'UTR

3 pEVL547 [*Prgef-1*::signal peptide : human wt PS-1 :: *unc-54* 3'UTR]

4 pEVL548 [*Prgef-1*::signal peptide : human L166P PS-1 :: *unc-54* 3'UTR]

5 pEVL549 [*Prgef-1*::signal peptide : human V44F I45F C99APP :: *unc-54* 3'UTR]

6 pEVL554 [*Prgef-1*::signal peptide : human V50F M51F C99APP :: *unc-54* 3'UTR]

Full sequences of the transgenes are provided as a supplementary file.

C. elegans maintenance and transgenesis

Animals were maintained on nematode growth medium (NGM) plates and fed *E. coli* OP50.[72] Transgenic lines were obtained by injecting human constructs with co-injection marker into gonads of *juIs1* [*Punc-25*::SNB-1::GFP]. Specifically, a mix of human APP variant (8-10 ng/μl) and/ or human PS-1 variant (8-10 ng/μl) plus marker *rol-6* (60.8 ng/μl) was injected into *juIs1* animals, subsequently selecting for animals displaying the roller phenotype.

Strains generated in this study:

wt C99APP + wt PS-1	*lhEx661*
I45F C99APP + wt PS-1	*lhEx655*
I45F C99APP	*lhEx648*
V44F I45F C99APP + wt PS-1	*lhEx650*
V44F I45F C99APP	*lhEx652*
V50F M51F C99APP + wt PS-1	*lhEx663*
wt C99APP + L166P PS-1	*lhEx657*
L166P PS-1	*lhEx659*

C. elegans lifespan analysis

Lifespan experiments were performed by selecting L4 animals from a plate that contains mixed stage animals. Animals were transferred to fresh plates whenever necessary to avoid contamination with animals of successive generations. Animals were maintained at 20 ^{o}C and were checked for survival at least once in two days. Animals that did not move when prodded were considered dead. Survival curves, calculation of median lifespan and statistical analysis were performed in 'Sigmaplot' using Kaplan Meier (log-rank test) method.

C. elegans microscopy and image analysis

L4 animals were selected and were maintained at 20 ºC. Adult worms from day 1 to day 7 and day 9 were scored for the number of SNB-1::GFP puncta in the ventral and dorsal nerve cords. Adult animals were anesthetized using 0.5% 2-phenoxypropanol in M9 and mounted on 2% agarose pads. Imaging was done using Olympus FV1000 laser scanning confocal microscope at 60X magnification NA 1.42. Image settings and acquisition parameters were optimized using Fluoview histogram function. All images were subsequently acquired using identical parameters. Specific acquisition parameters for each image are saved in the Olympus Image Format metadata.

C. elegans were also imaged in the Microscopy and Analytical Imaging Resource Core Laboratory (RRID:SCR_021801) at The University of Kansas using a TCS SPE Laser Scanning Confocal Upright Microscope (Leica Microsystems, DM6-Q model), with the 488 nm laser line, a Leica 63X/1.3NA ACS APO oil objective, 12-bit spectral PMT detector and a Leica LAS X Imaging software (version 3.5.7.23225). Synaptic puncta signal were detected using 488 nm excitation, 500-520 nm emission range. Images were captured at 1024 x 1024-pixel resolution, no bidirectional scanning, and a zoom factor at 1.0.

Confocal images were processed by using Fiji (ImageJ) software.[75] Fluorescent confocal images were opened with Fiji, and the series of slices for each image were stacked by 'Z-project'. Each stacked image was then converted to binary image.[76] A threshold value is then identified for each image to resolve individual synaptic punctum, also ensuring all puncta are included in the range by noticing the correspondence with visually evident puncta. While applying the threshold for ventral cord, cell bodies or any nonspecific background fluorescent objects are excluded from the analysis. Particles within the size range of 0.2 - □ (micron^2) were included in the analysis, excluding any that were on the edges along both axes using "Analyze Particle" command in ImageJ. As a result, the location (x,y coordinates) of every

puncta was obtained automatically. These values were exported to MS-Excel. Average number of synaptic puncta per 100 µm is determined by calculating the distance between two adjacent puncta along the x-axis. Graphs were plotted using GraphPad Prism 9 software. ANOVA was performed in this software, and significance for all possible pairwise comparisons were calculated using a Tukey's multiple comparisons test. For all statistical measurements, a threshold of adjusted P value <0.05 was set to determine significance in multiple comparison tests. (ns for P > 0.05, * for P ≤ 0.05, ** for P ≤ 0.01, *** for P ≤ 0.001, **** for P ≤ 0.0001).

QUANTIFICATION AND STATISTICAL ANALYSIS

General

All statistical methods for experiments are described in the respective figure legends. All calculations of significance were determined using either GraphPad Prism 9 or Microsoft Excel. Significance was determined by a p value of < 0.05, and annotated as * for P ≤ 0.05, ** for P ≤ 0.01, *** for P ≤ 0.001, **** for P ≤ 0.0001.

AICD-Flag production

AICD densitometry was carried out using Azurespot (Azure Biosystems). A standard curve established from a concentration range of C100-FLAG protein was used to calculate AICD-FLAG product concentration from the enzyme reaction mixtures. Unpaired two-tailed T-tests were used to compare measurements from FAD-mutant samples to those of WT samples.

Aβ40 and Aβ42 production

Aβ40 and Aβ42 levels were measured with specific ELISA kits from Invitrogen according to the manufacturer's instructions. Quantification was conducted using a Biotek Epoc 2 microplate reader. Unpaired two-tailed T-tests were used to compare measurements from FAD-mutant samples to those of WT samples.

Small peptide co-products

Tri- and tetrapeptide co-products of C100-Flag processing by γ-secretase were quantified by LC-MS/MS. To obtain a peptide chromatographic area, the signals from the 3 most abundant ions were summed using an ion mass width of 0.02 unit. Data were acquired in "V" mode. A standard curve for synthetic forms of each small peptide co-product was generated to use for quantification of test samples. Unpaired two-tailed T-tests were used to compare measurements from FAD-mutant samples to those of WT samples.

Resolution estimate of cryo-EM maps

The local resolution map was calculated using RELION 3.0.[57] Resolution estimations of all cryo-EM maps are based on the Fourier Shell Correlation (FSC) value of 0.143.[56]

Root-mean-square fluctuations in simulations

Root-mean-square fluctuations (RMSFs) of PS1 and substrate within the γ-secretase complexes were calculated by averaging the RMSFs calculated from individual PepGaMD simulations of each γ-secretase system. Changes in the RMSFs (ΔRMSF) from the WT to PS1 FAD mutant γ-

secretase were calculated by subtracting the RMSFs of the WT from those of PS1 FAD mutant γ-secretase.

Free energy calculations

The PyReweighting[70] toolkit was applied for free energy calculations from the D257-D385 and D385-V46 distances for each system.

Fluorescence lifetime imaging microscopy (FLIM)

Fluorescence emissions were collected using the ET525/50m-2p filter (Chroma Technology Corp, Bellows Falls, VT). The donor Alexa Fluor™ 488 lifetime was recorded using a high-speed photomultiplier tube (MCP R3809; Hamamatsu photonics, Hamamatsu City, Japan) and a time-correlated single-photon counting acquisition board (SPC-830; Becker & Hickl GmbH, Berlin, Germany). The acquired FLIM data were analyzed using SPC Image software (Becker & Hickl GmbH). Pseudo-colored images corresponding to the ratios of 6E10-Alexa Fluor™ 488 over C99-720 emission were generated in MATLAB (MathWorks, Natick, MA). For all graphs, n = 136-141 regions of interest (ROIs) from 7-10 cells, one-way ANOVA and the Tukey's multiple comparisons test.

***C. elegans* lifespan**

Animals were maintained at 20 ^{o}C and were checked for survival at least once in two days. Animals that did not move when prodded were considered dead. Survival curves, calculation of

median lifespan and statistical analysis were performed in Sigmaplot using Kaplan Meier (log-rank test) method.

C. elegans synaptic puncta

Synaptic puncta signal were detected using 488 nm excitation, 500-520 nm emission range. Images were captured at 1024 x 1024-pixel resolution, no bidirectional scanning, and a zoom factor at 1.0. Fluorescent confocal images were opened with Fiji (ImageJ), and the series of slices for each image were stacked by 'Z- project'. Each stacked image was then converted to binary image. A threshold value was then identified for each image to resolve individual synaptic punctum. Details for threshold setting and puncta counting are described above in *C. elegans* Microscopy and Image Analysis. Average number of synaptic puncta per 100 μm was determined by calculating the distance between two adjacent puncta along the x-axis. ANOVA was performed using GraphPad Prism 9 software, and significance for all possible pairwise comparisons were calculated using a Tukey's multiple comparisons test.

REFERENCES

1. Hardy, J., and Allsop, D. (1991). Amyloid deposition as the central event in the aetiology of Alzheimer's disease. Trends Pharmacol Sci *12*, 383-388.

2. Selkoe, D.J. (1991). The molecular pathology of Alzheimer's disease. Neuron *6*, 487-498.

3. Selkoe, D.J., and Hardy, J. (2016). The amyloid hypothesis of Alzheimer's disease at 25 years. EMBO Mol Med *8*, 595-608.

4. Benilova, I., Karran, E., and De Strooper, B. (2012). The toxic Aβ oligomer and Alzheimer's disease: an emperor in need of clothes. Nat Neurosci *15*, 349-357.

5. Karran, E., and De Strooper, B. (2022). The amyloid hypothesis in Alzheimer disease: new insights from new therapeutics. Nat Rev Drug Discov *21*, 306-318.

6. van Dyck, C.H., Swanson, C.J., Aisen, P., Bateman, R.J., Chen, C., Gee, M., Kanekiyo, M., Li, D., Reyderman, L., Cohen, S., et al. (2022). Lecanemab in Early Alzheimer's Disease. N Eng J Med *388*, 1631-1632.

7. Liu, K.Y., and Howard, R. (2021). Can we learn lessons from the FDA's approval of aducanumab? Nat Rev Neurol *17*, 715-722.

8. Bateman, R.J., Aisen, P.S., De Strooper, B., Fox, N.C., Lemere, C.A., Ringman, J.M., Salloway, S., Sperling, R.A., Windisch, M., and Xiong, C. (2011). Autosomal-dominant Alzheimer's disease: a review and proposal for the prevention of Alzheimer's disease. Alzheimer Res Ther *3*, 1. 10.1186/alzrt59.

9. Morris, J.C., Weiner, M., Xiong, C., Beckett, L., Coble, D., Saito, N., Aisen, P.S., Allegri, R., Benzinger, T.L.S., Berman, S.B., et al. (2022). Autosomal dominant and sporadic late onset Alzheimer's disease share a common in vivo pathophysiology. Brain *145*, 3594-3607.

10. Takami, M., Nagashima, Y., Sano, Y., Ishihara, S., Morishima-Kawashima, M., Funamoto, S., and Ihara, Y. (2009). γ-Secretase: successive tripeptide and tetrapeptide release from the transmembrane domain of β-carboxyl terminal fragment. J Neurosci *29*, 13042-13052.

11. Devkota, S., Williams, T.D., and Wolfe, M.S. (2021). Familial Alzheimer's disease mutations in amyloid protein precursor alter proteolysis by γ-secretase to incrase amyloid β-peptides of >45 residues. J Biol Chem. *296*:100281.

12. Lu, P., Bai, X.C., Ma, D., Xie, T., Yan, C., Sun, L., Yang, G., Zhao, Y., Zhou, R., Scheres, S.H., and Shi, Y. (2014). Three-dimensional structure of human γ-secretase. Nature *512*, 166-170.

13. Sato, T., Dohmae, N., Qi, Y., Kakuda, N., Misonou, H., Mitsumori, R., Maruyama, H., Koo, E.H., Haass, C., Takio, K., et al. (2003). Potential link between amyloid β-protein 42 and C-terminal fragment γ49-99 of β-amyloid precursor protein. J Biol Chem *278*, 24294-24301.

14. Song, W., Nadeau, P., Yuan, M., Yang, X., Shen, J., and Yankner, B.A. (1999). Proteolytic release and nuclear translocation of Notch-1 are induced by presenilin-1 and impaired by pathogenic presenilin-1 mutations. Proc Natl Acad Sci USA *96*, 6959-6963.

15. Schroeter, E.H., Ilagan, M.X., Brunkan, A.L., Hecimovic, S., Li, Y.M., Xu, M., Lewis, H.D., Saxena, M.T., De Strooper, B., Coonrod, A., et al. (2003). A presenilin dimer at the core of the γ-secretase enzyme: insights from parallel analysis of Notch 1 and APP proteolysis. Proc Natl Acad Sci USA *100*, 13075-13080.

16. Bentahir, M., Nyabi, O., Verhamme, J., Tolia, A., Horre, K., Wiltfang, J., Esselmann, H., and De Strooper, B. (2006). Presenilin clinical mutations can affect γ-secretase activity by different mechanisms. J Neurochem *96*, 732-742.

17. Bhattarai, S., Devkota, S., Meneely, K.M., Xing, M., Douglas, J.T., and Wolfe, M.S. (2020). Design of Substrate Transmembrane Mimetics as Structural Probes for γ-Secretase. J Am Chem Soc *142*, 3351-3355.

18. Bhattarai, S., Devkota, S., and Wolfe, M.S. (2021). Design of Transmembrane Mimetic Structural Probes to Trap Different Stages of γ-Secretase-Substrate Interaction. J Med Chem *64*, 15367-15378.

19. Esler, W.P., Das, C., and Wolfe, M.S. (2004). Probing pockets S2-S4' of the γ-secretase active site with (hydroxyethyl)urea peptidomimetics. Bioorg Med Chem Lett *14*, 1935-1938.

20. Das, C., Berezovska, O., Diehl, T.S., Genet, C., Buldyrev, I., Tsai, J.Y., Hyman, B.T., and Wolfe, M.S. (2003). Designed helical peptides inhibit an intramembrane protease. J Am Chem Soc *125*, 11794-11795.

21. Kornilova, A.Y., Bihel, F., Das, C., and Wolfe, M.S. (2005). The initial substrate-binding site of γ-secretase is located on presenilin near the active site. Proc Natl Acad Sci USA *102*, 3230-3235.

22. Zhou, R., Yang, G., Guo, X., Zhou, Q., Lei, J., and Shi, Y. (2019). Recognition of the amyloid precursor protein by human γ-secretase. Science *363*, eaaw0930

23. Fujinaga, M., Chernaia, M.M., Tarasova, N.I., Mosimann, S.C., and James, M.N. (1995). Crystal structure of human pepsin and its complex with pepstatin. Protein Sci *4*, 960-972.

24. Hong, L., Turner, R.T., 3rd, Koelsch, G., Shin, D., Ghosh, A.K., and Tang, J. (2002). Crystal structure of memapsin 2 (β-secretase) in complex with an inhibitor OM00-3. Biochemistry *41*, 10963-10967.

25. Kim, E.E., Baker, C.T., Dwyer, M.D., Murcko, M.A., Rao, B.G., Tung, R.D., and Navia, M.A. (1995). Crystal structure of HIV-1 protease in complex with VX-478, a potent and orally bioavailable inhibitor of the enzyme. J Am Chem Soc *117*, 1181-1182.

26. Bhattarai, A., Devkota, S., Bhattarai, S., Wolfe, M.S., and Miao, Y. (2020). Mechanisms of γ-Secretase Activation and Substrate Processing. ACS Cent Sci *6*, 969-983.

27. Bhattarai, A., Devkota, S., Do, H.N., Wang, J., Bhattarai, S., Wolfe, M.S., and Miao, Y. (2022). Mechanism of Tripeptide Trimming of Amyloid β-Peptide 49 by γ-Secretase. J Am Chem Soc *144*, 6215-6226. 10.1021/jacs.1c10533.

28. Do, H.N., Devkota, S., Bhattarai, A., Wolfe, M.S., and Miao, Y. (2023). Effects of presenilin-1 familial Alzheimer's disease mutations on γ-secretase activation for cleavage of amyloid precursor protein. Commun Biol *6*, 174.

29. Elangovan, M., Day, R.N., and Periasamy, A. (2002). Nanosecond fluorescence resonance energy transfer-fluorescence lifetime imaging microscopy to localize the protein interactions in a single living cell. J Microsc *205*, 3-14.

30. Liu, L., Lauro, B.M., Wolfe, M.S., and Selkoe, D.J. (2021). Hydrophilic loop 1 of Presenilin-1 and the APP GxxxG transmembrane motif regulate γ-secretase function in generating Alzheimer-causing Aβ peptides. J Biol Chem. *296*:100393.

31. Maesako, M., Houser, M.C.Q., Turchyna, Y., Wolfe, M.S., and Berezovska, O. (2022). Presenilin/γ-Secretase Activity Is Located in Acidic Compartments of Live. J Neurosci *42*, 145-154.

32. McKendell, A.K., Houser, M.C.Q., Mitchell, S.P.C., Wolfe, M.S., Berezovska, O., and Maesako, M. (2022). In-Depth Characterization of Endo-Lysosomal Aβ in Intact Neurons. Biosensors *12*, 663.

33. Levitan, D., Doyle, T.G., Brousseau, D., Lee, M.K., Thinakaran, G., Slunt, H.H., Sisodia, S.S., and Greenwald, I. (1996). Assessment of normal and mutant human presenilin function in Caenorhabditis elegans. Proc Natl Acad Sci USA *93*, 14940-14944.

34. Baumeister, R., Leimer, U., Zweckbronner, I., Jakubek, C., Grünberg, J., and Haass, C. (1997). Human presenilin-1, but not familial Alzheimer's disease (FAD) mutants, facilitate *Caenorhabditis elegans* Notch signalling independently of proteolytic processing. Genes and Function *1*, 149-159.

35. Guerreiro, R.J., Baquero, M., Blesa, R., Boada, M., Bras, J.M., Bullido, M.J., Calado, A., Crook, R., Ferreira, C., Frank, A., et al. (2010). Genetic screening of Alzheimer's disease genes in Iberian and African samples yields novel mutations in presenilins and APP. Neurobiol Aging *31*, 725-731.

36. Lichtenthaler, S.F., Wang, R., Grimm, H., Uljon, S.N., Masters, C.L., and Beyreuther, K. (1999). Mechanism of the cleavage specificity of Alzheimer's disease γ-secretase identified by phenylalanine-scanning mutagenesis of the transmembrane domain of the amyloid precursor protein. Proc Natl Acad Sci USA *96*, 3053-3058.

37. Bolduc, D.M., Montagna, D.R., Seghers, M.C., Wolfe, M.S., and Selkoe, D.J. (2016). The amyloid-beta forming tripeptide cleavage mechanism of γ-secretase. eLife *5*, pii: e17578.

38. Pope, C.A., Wilkins, H.M., Swerdlow, R.H., and Wolfe, M.S. (2021). Mutations in the Amyloid-β Protein Precursor Reduce Mitochondrial Function and Alter Gene Expression Independent of 42-Residue Amyloid-β Peptide. J Alzheimer Dis *83*, 1039-1049.

39. Moehlmann, T., Winkler, E., Xia, X., Edbauer, D., Murrell, J., Capell, A., Kaether, C., Zheng, H., Ghetti, B., Haass, C., and Steiner, H. (2002). Presenilin-1 mutations of leucine 166 equally affect the generation of the Notch and APP intracellular domains independent of their effect on Aβ42 production. Proc Natl Acad Sci USA *99*, 8025-8030.

40. Makin, S. (2018). The amyloid hypothesis on trial. Nature *559*, S4-S7.

41. Kepp, K.P., Robakis, N.K., Høilund-Carlsen, P.F., Sensi, S.L., and Vissel, B. (2023). The amyloid cascade hypothesis: an updated critical review. Brain 10.1093/brain/awad159.

42. Szaruga, M., Munteanu, B., Lismont, S., Veugelen, S., Horre, K., Mercken, M., Saido, T.C., Ryan, N.S., De Vos, T., Savvides, S.N., et al. (2017). Alzheimer's-Causing Mutations Shift Aβ Length by Destabilizing γ-Secretase-Abeta$_n$ Interactions. Cell *170*, 443-456 e414.

43. Sun, L., Zhou, R., Yang, G., and Shi, Y. (2017). Analysis of 138 pathogenic mutations in presenilin-1 on the in vitro production of Aβ42 and Aβ40 peptides by γ-secretase. Proc Natl Acad Sci USA *114*, E476-E485.

44. Leng, F., and Edison, P. (2021). Neuroinflammation and microglial activation in Alzheimer disease: where do we go from here? Nat Rev Neurol *17*, 157-172.

45. https://www.proteinatlas.org/ENSG00000142192-APP/tissue.

46. Cole, S.L., and Vassar, R. (2008). The role of APP processing by BACE1, the β-secretase, in Alzheimer's disease pathophysiology. J Biol Chem *283*, 29621-29625.

47. Shen, J., and Kelleher, R.J., 3rd (2007). The presenilin hypothesis of Alzheimer's disease: evidence for a loss-of-function pathogenic mechanism. Proc Natl Acad Sci USA *104*, 403-409.

48. Wang, B., Yang, W., Wen, W., Sun, J., Su, B., Liu, B., Ma, D., Lv, D., Wen, Y., Qu, T., et al. (2010). γ-Secretase gene mutations in familial acne inversa. Science *330*, 1065.

49. Yip, M.C.J., and Shao, S. (2021). Detecting and Rescuing Stalled Ribosomes. Trends Biochem Sci *46*, 731-743.

50. Ledesma, M.D., Martin, M.G., and Dotti, C.G. (2012). Lipid changes in the aged brain: effect on synaptic function and neuronal survival. Prog Lipid Res *51*, 23-35.

51. Li, Y.M., Lai, M.T., Xu, M., Huang, Q., DiMuzio-Mower, J., Sardana, M.K., Shi, X.P., Yin, K.C., Shafer, J.A., and Gardell, S.J. (2000). Presenilin 1 is linked with γ-secretase activity in the detergent solubilized state. Proc Natl Acad Sci USA *97*, 6138-6143.

52. Bolduc, D.M., Selkoe, D.J., and Wolfe, M.S. (2017). Enzymatic Assays for Studying Intramembrane Proteolysis. Methods Enzymol *584*, 295-308.

53. Fraering, P.C., Ye, W., Strub, J.M., Dolios, G., LaVoie, M.J., Ostaszewski, B.L., Van Dorsselaer, A., Wang, R., Selkoe, D.J., and Wolfe, M.S. (2004). Purification and Characterization of the Human γ-Secretase Complex. Biochemistry *43*, 9774-9789.

54. Osenkowski, P., Li, H., Ye, W., Li, D., Aeschbach, L., Fraering, P.C., Wolfe, M.S., Selkoe, D.J., and Li, H. (2009). Cryoelectron microscopy structure of purified γ-secretase at 12 Å resolution.

55. Bhattarai, S., Liu, L., and Wolfe, M.S. (2021). Discovery of aryl aminothiazole γ-secretase modulators with novel effects on amyloid β-peptide production. Bioorg Med Chem Lett *54*, 128446. 10.1016/j.bmcl.2021.128446.

56. Rosenthal, P.B., and Henderson, R. (2003). Optimal determination of particle orientation, absolute hand, and contrast loss in single-particle electron cryomicroscopy. J Mol Biol *333*, 721-745.

57. Luo, Z., Campos-Acevedo, A.A., Lv, L., Wang, Q., and Ma, J. (2021). Sparseness and Smoothness Regularized Imaging for improving the resolution of Cryo-EM single-particle reconstruction. Proc Natl Acad Sci USA *118*, 10.1073/pnas.2013756118.

58. Do, H.N., Devkota, S., Bhattarai, A., Wolfe, M.S., and Miao, Y. (2023). Effects of presenilin-1 familial Alzheimer's disease mutations on γ-secretase activation for cleavage of amyloid precursor protein. Commun Biol *6,* 174.

59. Jo, S., Kim, T., Iyer, V., and Im, W. (2008). CHARMM-GUI: A Web-based Graphical User Interface for CHARMM. J Computat Chem *29*, 1859-1865.

60. Lee, J., Cheng, X., Swails, J., Yeom, M., Eastman, P., Lemkul, J., Wei, S., Buckner, J., Jeong, J., Qi, Y., et al. (2016). CHARMM-GUI Input Generator for NAMD, GROMACS, AMBER, OpenMM, and CHARMM/OpenMM Simulations using the CHARMM36 Additive Force Field. J Chem Theor Computat *12*, 405-413.

61. Wu, E., Cheng, X., Jo, S., Rui, H., Song, K., Davila-Contreras, E., Qi, Y., Lee, J., Monje-Galvan, V., Venable, R., et al. (2014). CHARMM-GUI Membrane Builder Toward Realistic Biological Membrane Simulations. J Computat Chem *35*, 1997-2004.

62. Jo, S., Kim, T., and Im, W. (2007). Automated Builder and Database of Protein/Membrane Complexes for Molecular Dynamics Simulations. PLoS ONE *2*, e880.

63. Bhattarai, A., Devkota, S., Do, H., Wang, J., Bhattarai, S., Wolfe, M., and Miao, Y. (2022). Mechanism of Tripeptide Trimming of Amyloid β-Peptide 49 by γ-Secretase. J Am Chem Soc *144*, 6215-6226.

64. Huang, J., Rauscher, S., Nawrocki, G., Ran, T., Feig, M., de Groot, B.L., Grubmuller, H., and MacKerell Jr, A.D. (2017). CHARMM36m: an improved force field for folded and intrinscially disordered proteins. Nat Methods *14*, 71-73.

65. Case, D.A., Belfon, K., Ben-Shalom, I.Y., Brozell, S.R., Cerutti, D.S., Cheatham, T.E., Cruzeiro, V.W.D., Darden, T., Duke, R.E., and Giambasu, G. (2020). AMBER 2020.

66. Wang, J., and Miao, Y. (2020). Peptide Gaussian accelerated molecular dynamics (Pep-GaMD): enhanced sampling and free energy and kinetics calculations of peptide binding. J Chem Phys *153*, 154109.

67. Miao, Y., Feher, V.A., and McCammon, J.A. (2015). Gaussian accelerated molecular dynamics: unconstrained enhanced sampling and free energy calculation. J Chel Theor Computat *11*, 3584-3595.

68. Humphrey, W., Dalke, A., and Schulten, K. (1996). VMD: visual molecular dynamics. J Mol Graph Model *14*, 33-38.

69. Roe, D.R., and Cheatham, I.T.E. (2013). PTRAJ and CPPTRAJ: software for processing and analysis of molecular dynamics trajectory data. J Chem Theor Computat *9*, 3084-3095.

70. Miao, Y., Sinko, W., Pierce, L., Bucher, D., Walker, R.C., and McCammon, J.A. (2014). Improved reweighting of accelerated molecular dynamics simulations for free energy calculation. J Chem Theor Computat *10*, 2677-2689.

71. Houser, M.C., Hou, S.S., Perrin, F., Turchyna, Y., Bacskai, B.J., Berezovska, O., and Maesako, M. (2020). A Novel NIR-FRET Biosensor for Reporting PS/γ-Secretase Activity in Live Cells. Sensors *20*, 10.3390/s20215980.

72. Brenner, S. (1974). The genetics of Caenorhabditis elegans. Genetics *77*, 71-94.

73. Hallam, S.J., and Jin, Y. (1998). lin-14 regulates the timing of synaptic remodelling in Caenorhabditis elegans. Nature *395*, 78-82.

74. Aquino Nunez, W., Combs, B., Gamblin, T.C., and Ackley, B.D. (2022). Age-dependent accumulation of tau aggregation in Caenorhabditis elegans. Front Aging *3*, 928574. 10.3389/fragi.2022.928574.

75. Schindelin, J., Arganda-Carreras, I., Frise, E., Kaynig, V., Longair, M., Pietzsch, T., Preibisch, S., Rueden, C., Saalfeld, S., Schmid, B., et al. (2012). Fiji: an open-source platform for biological-image analysis. Nat Methods *9*, 676-682.

76. Huarcaya Najarro, E., and Ackley, B.D. (2013). C. elegans fmi-1/flamingo and Wnt pathway components interact genetically to control the anteroposterior neurite growth of the VD GABAergic neurons. Dev Biol *377*, 224-235.

KEY RESOURCES TABLE

REAGENT or RESOURCE	SOURCE	IDENTIFIER
Antibodies		
Mouse anti-Flag M2	Sigma-Aldrich	Cat. No. F1804; RRID Ab_262044
Mouse anti-FLAG M2-agarose beads	Sigma-Aldrich	Cat. No. A2220; RRID:AB_10063035
Mouse anti-GAPDH	Cell Signaling Technology	Cat. No. 97166; RRID:AB_2756824
Mouse anti-PSEN1-NTF	Bio-Legend	Cat. No. 823401; RRID:AB_2564868
Mouse anti-Aβ 6E10	Bio-Legend	Cat. No. 803001; RRID:AB_2564653
Rabbit anti-total Aβ	Cell Signaling Technology	Cat. No. 8243; RRID:AB_2797642
Rabbit anti-nicastrin	Novus Biologicals	Cat. No. NBP2-57365
Rabbit anti-PSEN1 Loop (EP2000Y)	Abcam	Cat. No. ab76083; RRID:AB_1310605
Alexa Fluor™ 488-conjugated goat anti-mouse IgG	ThermoFisher	Cat. No. A32723; RRID:AB_2633275
Cy3-conjugated goat anti-rabbit IgG	ThermoFisher	Cat. No. A10520; RRID:AB_2534029
Bacterial and virus strains		
E. coli BL21 DE3	New England Biolabs	Cat. No. C2530H
Biological samples		
Chemicals, peptides, and recombinant proteins		
FreeStyle™ 293 Expression Medium	ThermoFisher	Cat. No. 12338018
^{13}C glucose	Cambridge Isotope Laboratories	Cat. No. CLM-1396
$^{15}NH_4Cl$	Cambridge Isotope Laboratories	Cat. No. NLM-467
Pac1 restriction enzyme	New England Biolabs	Cat. No. R0547S
Swa1 restriction enzyme	New England Biolabs	Cat. No. R0604S
BamH1 restriction enzyme	New England Biolabs	Cat. No. R01365
NgoM4 restriction enzyme	New England Biolabs	Cat. No. R05645
DOPC (1,2-dioleoyl-*sn*-glycerol-3-phosphocholine)	Avanti Polar Lipids	Cat. No. 850375

DOPE (1,2-dioleoyl-*sn*-glycero-3-phosphoethanolamine)	Avanti Polar Lipids	Cat. No. 850725
CHAPSO (3-[(3-cholamidopropyl) dimethylammonio]-2-hydroxy-1-propanesulfonate)	MP Biomedicals	Cat. No. 190320
Digitonin	Goldbio	Cat. No. D-180-5
Transmembrane substrate mimetic inhibitor SB-250	In-house	Ref. 18, cmpd 28
Peptides VIT, ITL, VIV, TVI, IAT and VVIAA	New England Peptide	Custom synthesized
Critical commercial assays		
QuikChange Lightning Multi-Site Directed Mutagenesis kit	Agilent	Cat. No. 210513
Amyloid β-peptide 1-40 ELISA kit	Invitrogen	Cat. No. KHB3481
Amyloid β-peptide 1-40 ELISA kit	Invitrogen	Cat. No. KHB3441
Deposited data		
CryoEM map for the structure of γ-secretase bound to probe SB-250	This study	EMDB: EMD-36948
Atomic model for the structure of γ-secretase bound to probe SB-250	This study	PDB: 8K8E
Experimental models: Cell lines		
FreeStyle™ HEK293F cells	ThermoFisher	Cat. No. R79007
HEK293 cells	ATCC	Cat. No. CRL-1573
HEK293 cells stably expressing WT APP C99	This study	N/A
HEK293 cells stably expressing I45F APP C99	This study	N/A
HEK293 cells stably expressing V44F/I45F APP C99	This study	N/A
HEK293 cells with PSEN1/2 double knockout by CRISPR	Lei Liu, Brigham and Women's Hospital	Ref. 30
Experimental models: Organisms/strains		
C. elegans parental *juIs1* strain [unc-25p::snb-1::GFP + lin-15(+)]		Ref. 73
C. elegans juIs1 + wt C99APP + wt PS-1 (lhEx661)	This study	N/A
C. elegans juIs1 + I45F C99APP + wt PS-1 (lhEx655)	This study	N/A
C. elegans juIs1 + I45F C99APP (lhEx648)	This study	N/A
C. elegans juIs1 + V44F I45F C99APP + wt PS-1 (lhEx650)	This study	N/A
C. elegans juIs1 + V44F I45F C99APP (lhEx652)	This study	N/A
C. elegans juIs1 + V50F M51F C99APP + wt PS-1 (lhEx663)	This study	N/A
C. elegans juIs1 + wt C99APP + L166P PS-1 (lhEx657)	This study	N/A
C. elegans juIs1 + L166P PS-1 (lhEx659)	This study	N/A
Oligonucleotides		
DNA primers for P117L PSEN1 mutagenesis: ggcagctaatctataccctattcacagaagataccgagactg	Invitrogen	Custom synthesized
DNA primers for I143T PSEN1 mutagenesis: gccatcatgatcagtgtcactgttgtcatgactatcctcctg	Invitrogen	Custom synthesized

DNA primers for L166P PSEN1 mutagenesis: aaggtcatccatgcctggcctattatatcatctctattgctg	Invitrogen	Custom synthesized
DNA primers for G384A PSEN1 mutagenesis: ggagtaaaacttggattggcagatttcattttctacagtg	Invitrogen	Custom synthesized
DNA primers for L435F PSEN1 mutagenesis: aagaaagcattgccagcttttccaatctccatcacctttgggc	Invitrogen	Custom synthesized
DNA primers for L286V PSEN1 mutagenesis: gaaacgctttttccagctgtcatttactcctcaacaatggtg	Invitrogen	Custom synthesized
DNA inserts for plasmid construction and generation of transgenic *C. elegans* lines	GeneArt/ ThermoFisher	Custom synthesized; see Supplemental Table
Recombinant DNA		
pMLINK-PSEN1	Coauthor Y. Shi	Ref. 12
pMLINK-Aph1 (with C-terminal HA epitope tag)	Coauthor Y. Shi	Ref. 12
pMLINK-NCT (with C-terminal V5 and 6XHIS epitope tags)	Coauthor Y. Shi	Ref. 12
pMLINK-Pen-2 (with N-terminal STREP and FLAG epitope tags)	Coauthor Y. Shi	Ref. 12
pMLINK-PSEN1-Aph1-NCT-Pen-2	This study	Ref. 12
pMLINK-PSEN1(L166P)-Aph1-NCT-Pen-2	This study	N/A
pMLINK-PSEN1(G384A)-Aph1-NCT-Pen-2	This study	N/A
pMLINK-PSEN1(I143T)-Aph1-NCT-Pen-2	This study	N/A
pMLINK-PSEN1(L435P)-Aph1-NCT-Pen-2	This study	N/A
pMLINK-PSEN1(L286V)-Aph1-NCT-Pen-2	This study	N/A
pMLINK-PSEN1(P117L)-Aph1-NCT-Pen-2	This study	N/A
pET22b-C100-FLAG	In-house	Ref. 51
pCMV(puro)-C99 with APP signal sequence	Lei Liu, Brigham and Women's Hospital	Ref. 55
C99 miRFP720-miRFP670 (C99 720-670) biosensor	Coauthor M. Maesako	Ref. 71
pcDNA3.1-C99 miRFP720	This study	N/A
worm expression vector pEVL415 (P*rgef-1*:*htau40*::*gfp*::*unc-54* 3′UTR)	Co-author B. Ackley	Ref. 74
Software and algorithms		
Prism 9 version 9.5.1	GraphPad	https://www.graphpad.com
Sigmaplot for Windows v.14	Systat Software GmbH	http://www.systat.de/
Fiji ImageJ 1.53c	NIH	https://imagej.nih.gov/
AzureSpot	Azure Biosystems	https://azurebiosystems.com/
MassLynx	Waters	https://www.waters.com
RELION 3.0	https://www2.mrc-lmb.cam.ac.uk/relion	Ref. 57
CHARMM-GUI	https://www.charmm-gui.org/	Refs. 59-61

Peptide Gaussian accelerated molecular dynamics (Pep-GaMD)	Coauthor Y. Miao	Ref. 66
Amber 20	https://ambermd.org/	Ref. 65
VMD	https://www.ks.uiuc.edu/	Ref. 68
PyReweighting	Coauthor Y. Miao	Ref. 70
SPC-830 (fluorescence lifetime imaging microscopy data collection)	Becker & Hickl GmbH	https://www.becker-hickl.com
SPC Image software version 2.5 (fluorescence lifetime imaging microscopy analysis	Becker & Hickl GmbH	https://www.becker-hickl.com
MATLAB (pseudo-color fluorescence lifetime imaging microscopy)	MathWorks	https://www.mathworks.com/
LAS X Imaging software v3.5.7 (confocal microscopy of *C. elegans*)	Leica Microsystems	https://www.leica-microsystems.com/
Fluoview SW FV10 - ASW v. 4.00 (fluorescence microscopy of *C. elegans*)	Olympus Life Science	https://www.olympus-lifescience.com/
Other		

Figure 1

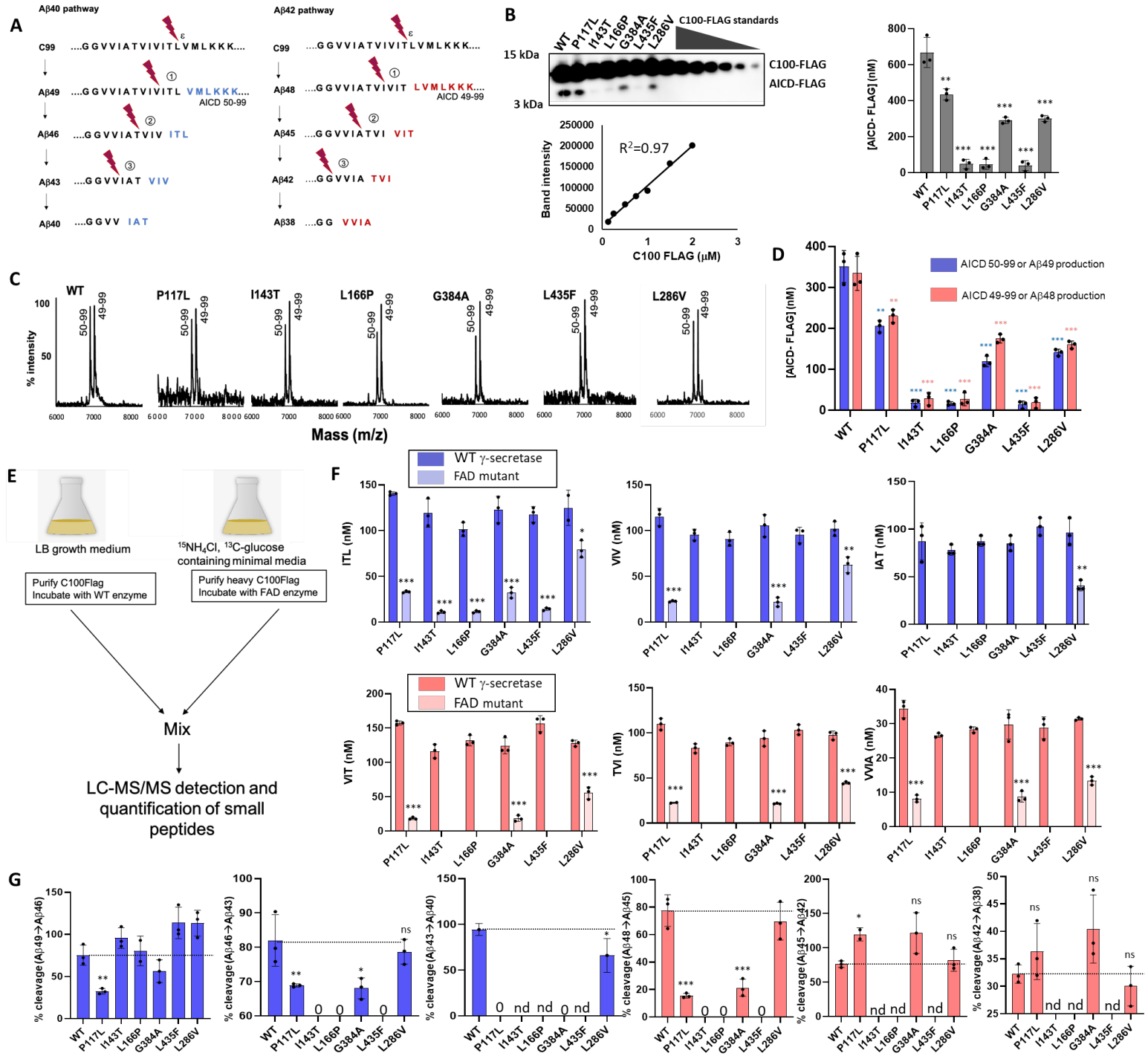
A
Aβ40 pathway
C99 ....GGVVIATVIVITLVMLKKK....
Aβ49 ....GGVVIATVIVITL VMLKKK....
AICD 50-99
Aβ46 ....GGVVIATVIV ITL
Aβ43 ....GGVVIAT VIV
Aβ40 ....GGVV IAT
Aβ42 pathway
C99 ....GGVVIATVIVITLVMLKKK....
Aβ48 ....GGVVIATVIVIT LVMLKKK....
AICD 49-99
Aβ45 ....GGVVIATVI VIT
Aβ42 ....GGVVIA TVI
Aβ38 ....GG VVIA
B
WT P117L I143T L166P G384A L435F L286V
C100-FLAG standards
15 kDa
3 kDa
C100-FLAG
AICD-FLAG
Band intensity
R2=0.97
C100 FLAG (μM)
[AICD- FLAG] (nM)
C
WT P117L I143T L166P G384A L435F L286V
% intensity
50-99
49-99
Mass (m/z)
D
AICD 50-99 or Aβ49 production
AICD 49-99 or Aβ48 production
[AICD- FLAG] (nM)
E
LB growth medium
15NH4Cl, 13C-glucose containing minimal media
Purify C100Flag
Incubate with WT enzyme
Purify heavy C100Flag
Incubate with FAD enzyme
Mix
LC-MS/MS detection and quantification of small peptides
F
WT γ-secretase
FAD mutant
ITL (nM)
VIV (nM)
IAT (nM)
VIT (nM)
TVI (nM)
VVIA (nM)
G
% cleavage (Aβ49→Aβ46)
% cleavage (Aβ46→Aβ43)
% cleavage (Aβ43→Aβ40)
% cleavage (Aβ48→Aβ45)
% cleavage (Aβ45→Aβ42)
% cleavage (Aβ42→Aβ38)
ns
nd

Figure 2

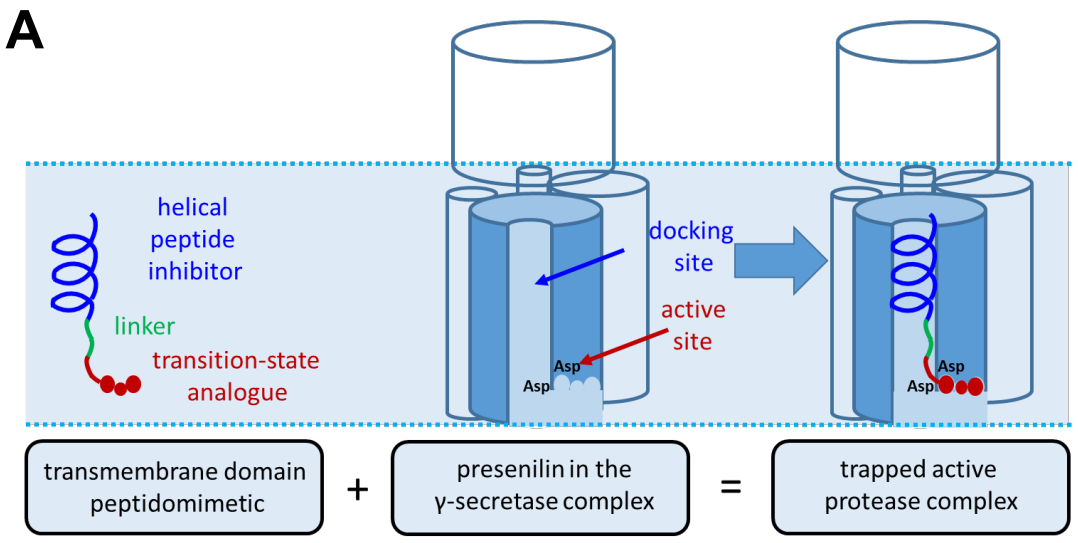
A
helical peptide inhibitor
linker
transition-state analogue
docking site
active site
Asp
Asp
transmembrane domain peptidomimetic
+
presenilin in the γ-secretase complex
=
trapped active protease complex
SB-250: Boc-Val-Gly-Aib-Val-Val-Ile-Aib-Phe-Val-Aib-Gly-Gly-Gly-Val-PheψPhe-Leu-Val-NH2

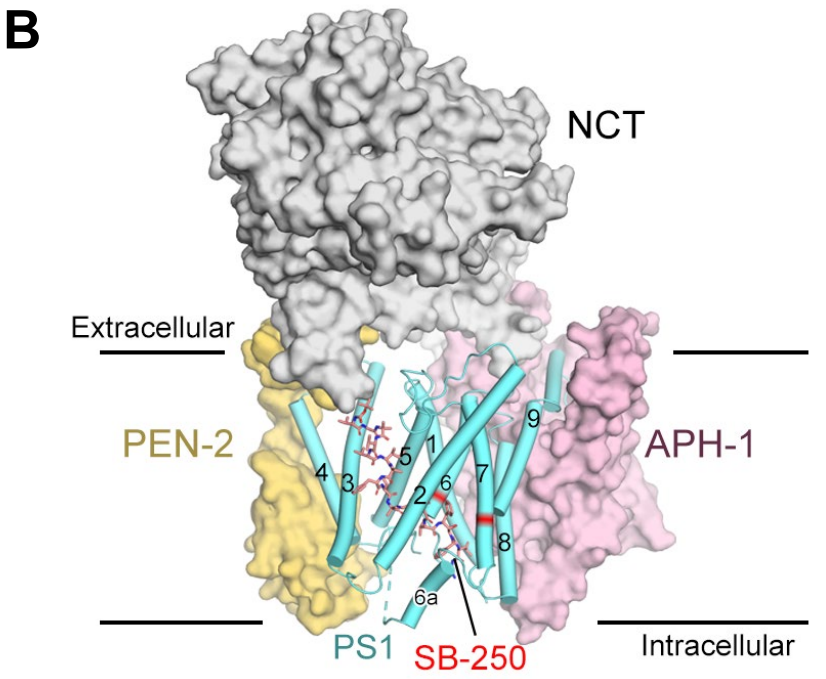
B
NCT
Extracellular
PEN-2
APH-1
PS1
SB-250
Intracellular

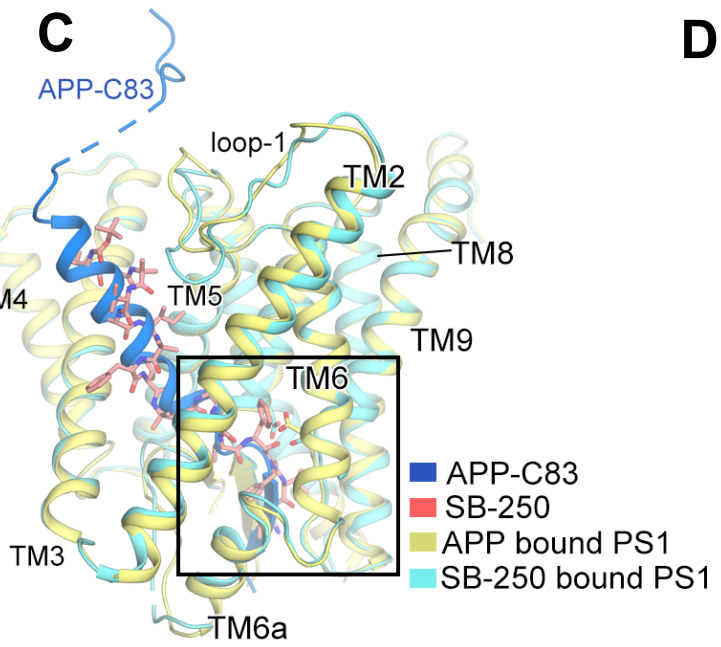
C
APP-C83
loop-1
TM2
TM8
TM4
TM5
TM9
TM6
TM3
TM6a
APP-C83
SB-250
APP bound PS1
SB-250 bound PS1

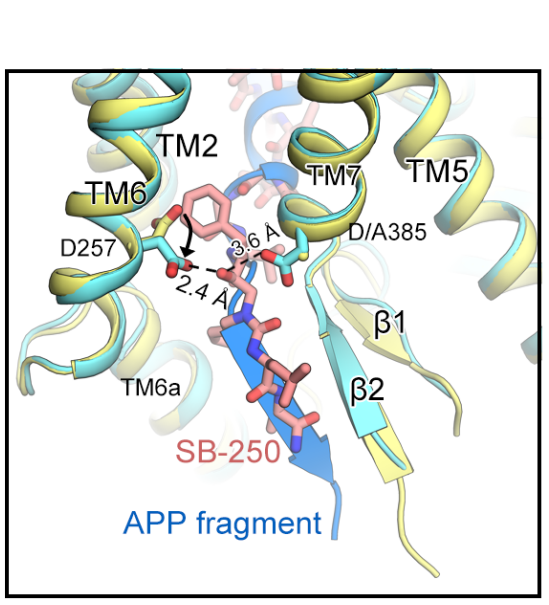
D
TM2
TM6
TM7
TM5
D257
D/A385
3.6 Å
2.4 Å
β1
β2
TM6a
SB-250
APP fragment

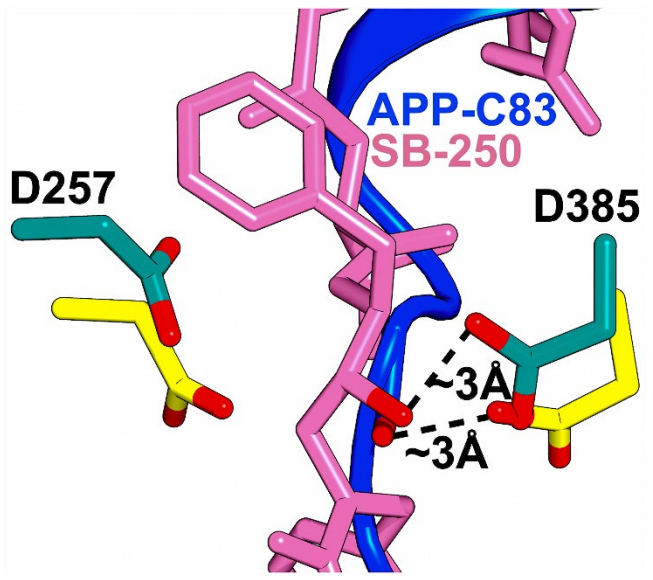
E
APP-C83
SB-250
D257
D385
~3Å
~3Å

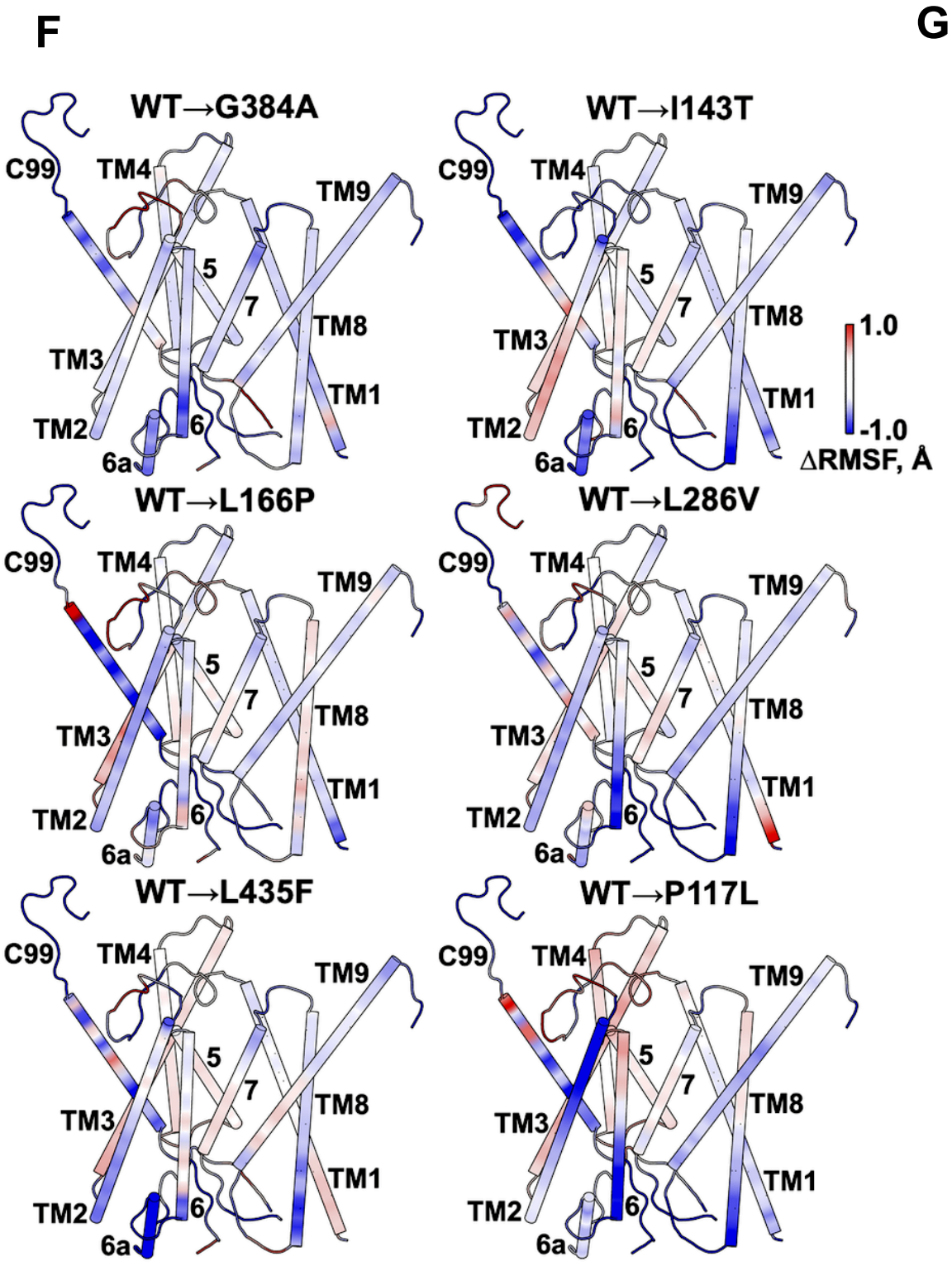
F
WT→G384A
WT→I143T
WT→L166P
WT→L286V
WT→L435F
WT→P117L
C99
TM4
TM9
TM8
TM3
TM1
TM2
6a
5
7
6
1.0
-1.0
ΔRMSF, Å

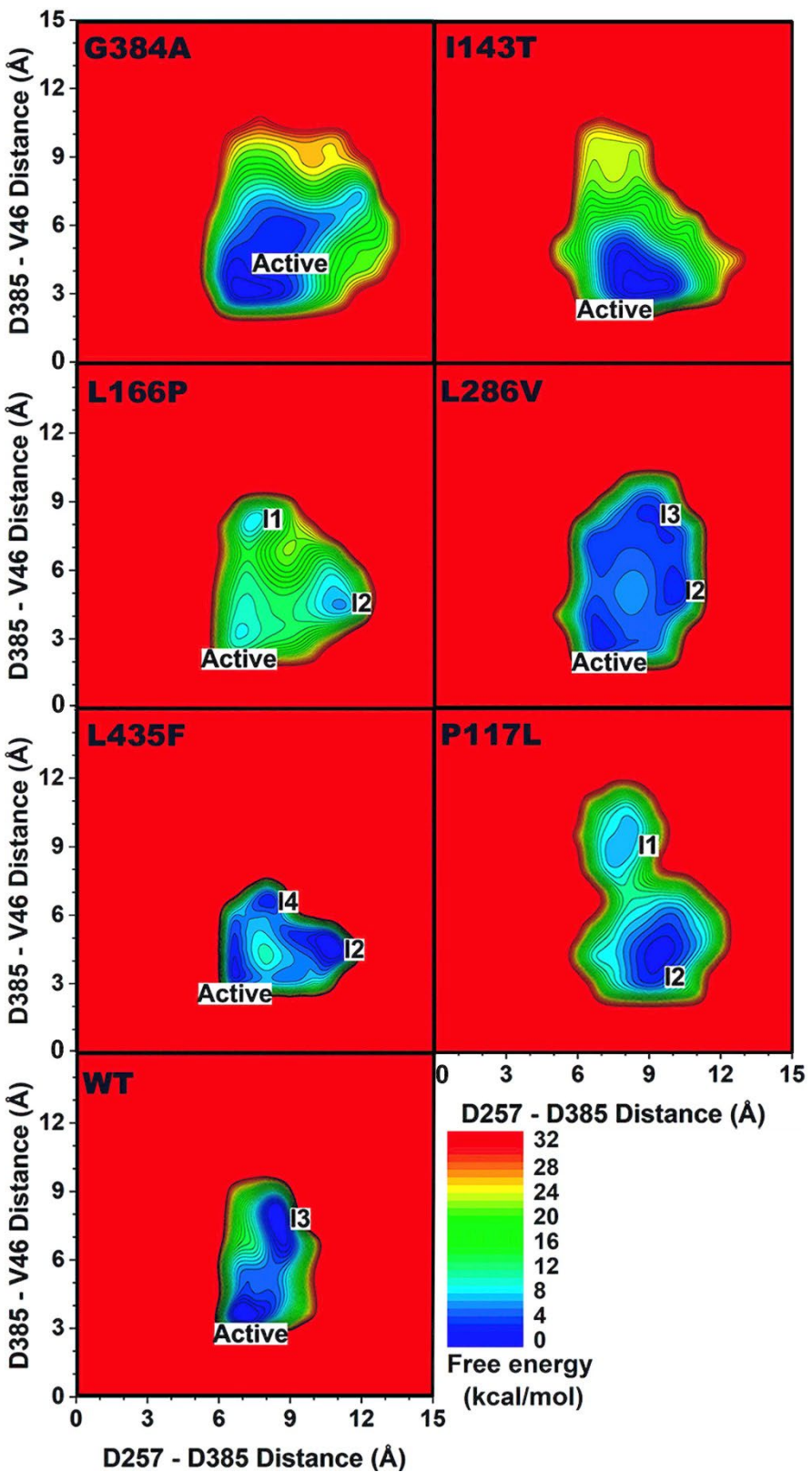
G
G384A
I143T
L166P
L286V
L435F
P117L
WT
Active
I1
I2
I3
I4
D385 - V46 Distance (Å)
D257 - D385 Distance (Å)
0
3
6
9
12
15
32
28
24
20
16
12
8
4
0
Free energy (kcal/mol)

Figure 3

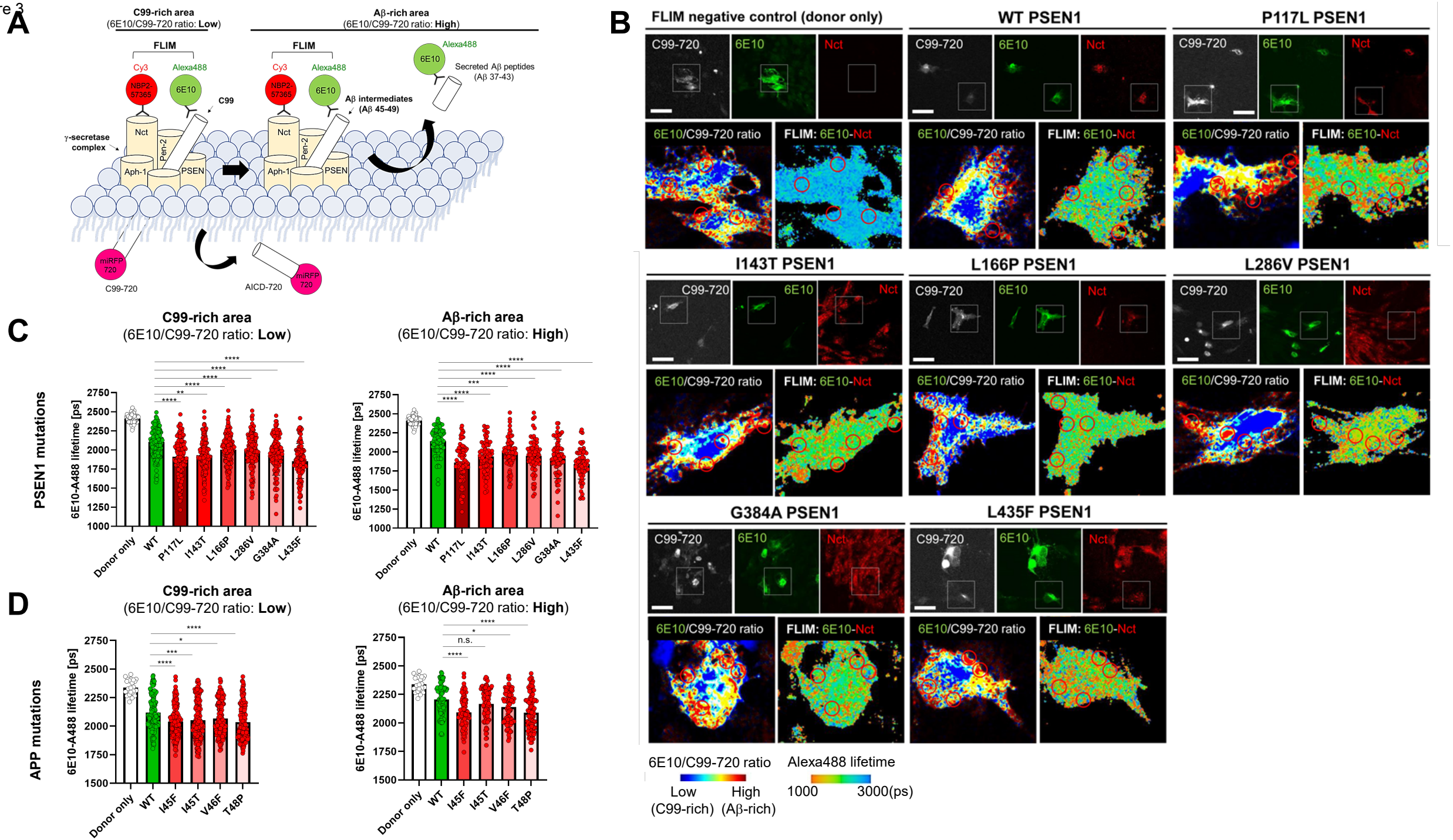
A
C99-rich area
(6E10/C99-720 ratio: Low)
Aβ-rich area
(6E10/C99-720 ratio: High)
FLIM
Cy3
Alexa488
NBP2-57365
6E10
C99
Aβ intermediates (Aβ 45-49)
Secreted Aβ peptides (Aβ 37-43)
γ-secretase complex
Nct
Pen-2
Aph-1
PSEN
miRFP 720
C99-720
AICD-720
B
FLIM negative control (donor only)
WT PSEN1
P117L PSEN1
I143T PSEN1
L166P PSEN1
L286V PSEN1
G384A PSEN1
L435F PSEN1
C99-720
6E10
Nct
6E10/C99-720 ratio
FLIM: 6E10-Nct
6E10/C99-720 ratio
Alexa488 lifetime
Low (C99-rich)
High (Aβ-rich)
1000
3000(ps)
C
C99-rich area
(6E10/C99-720 ratio: Low)
Aβ-rich area
(6E10/C99-720 ratio: High)
PSEN1 mutations
6E10-A488 lifetime [ps]
Donor only
WT
P117L
I143T
L166P
L286V
G384A
L435F
D
C99-rich area
(6E10/C99-720 ratio: Low)
Aβ-rich area
(6E10/C99-720 ratio: High)
APP mutations
6E10-A488 lifetime [ps]
Donor only
WT
I45F
I45T
V46F
T48P
n.s.

Figure 4

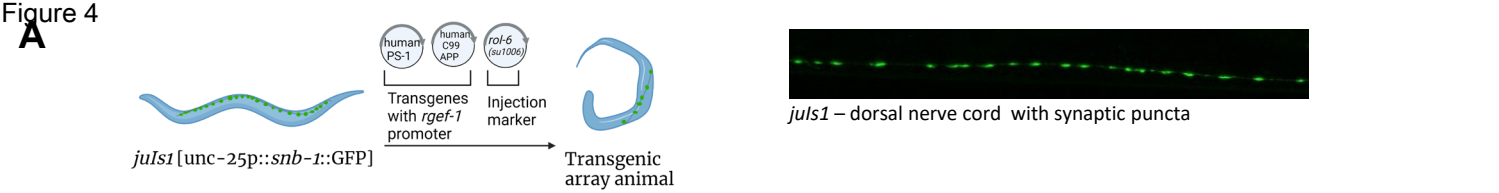

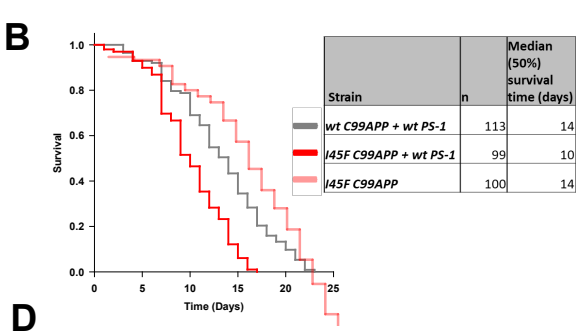

Strain	n	Median (50%) survival time (days)
wt C99APP + wt PS-1	113	14
I45F C99APP + wt PS-1	99	10
I45F C99APP	100	14

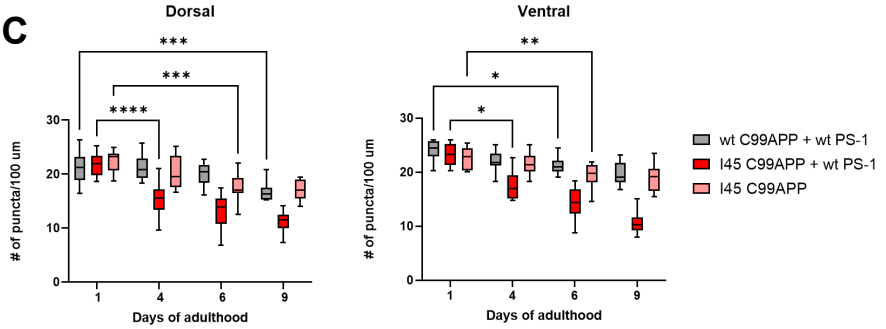

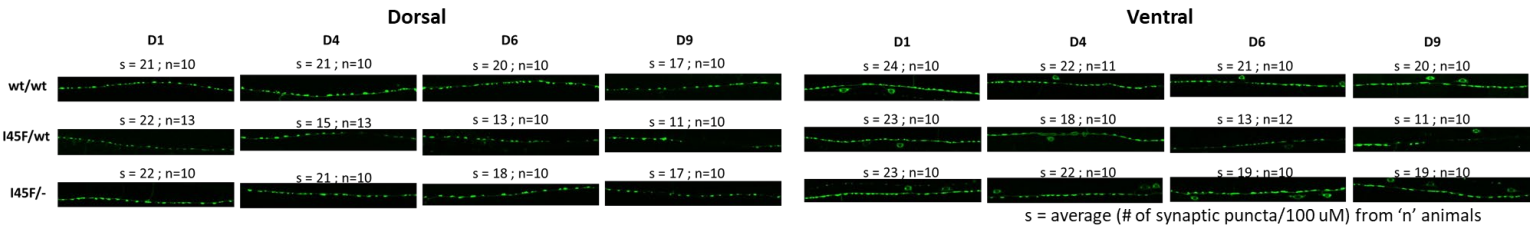

s = average (# of synaptic puncta/100 uM) from 'n' animals

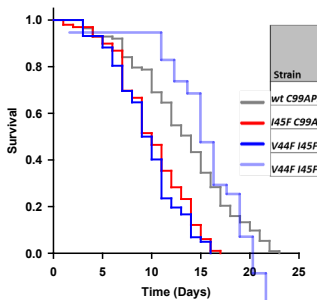

Strain	n	Median (50%) survival time (days)
wt C99APP + wt PS-1	113	14
I45F C99APP + wt PS-1	99	10
V44F I45F C99APP + wt PS-1	102	9
V44F I45F C99APP	102	12

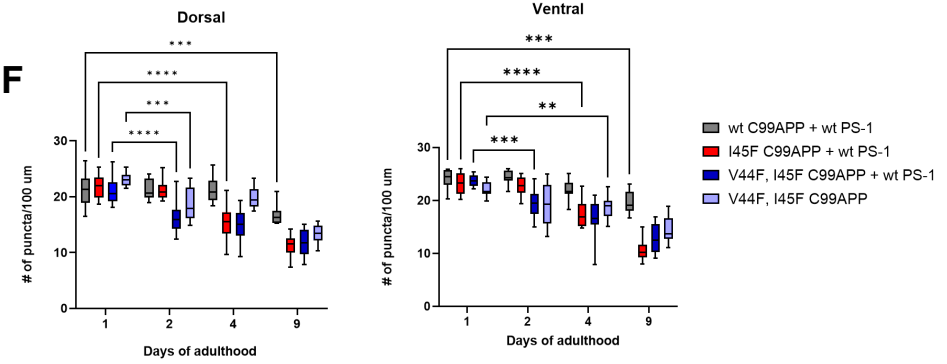

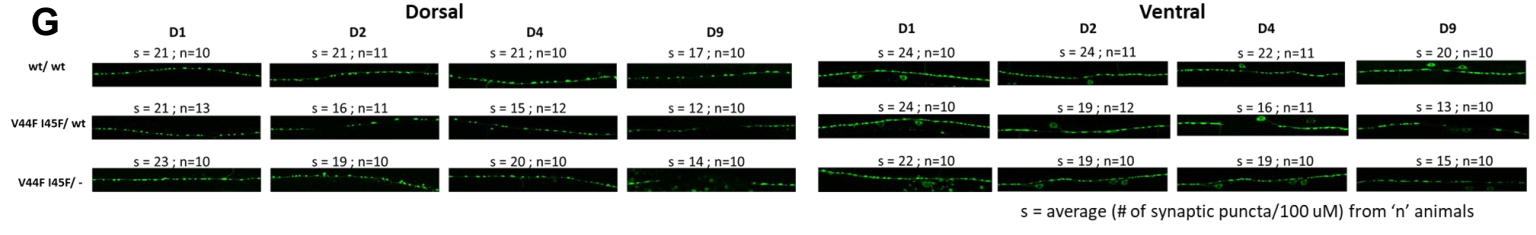

s = average (# of synaptic puncta/100 uM) from 'n' animals

Figure 5

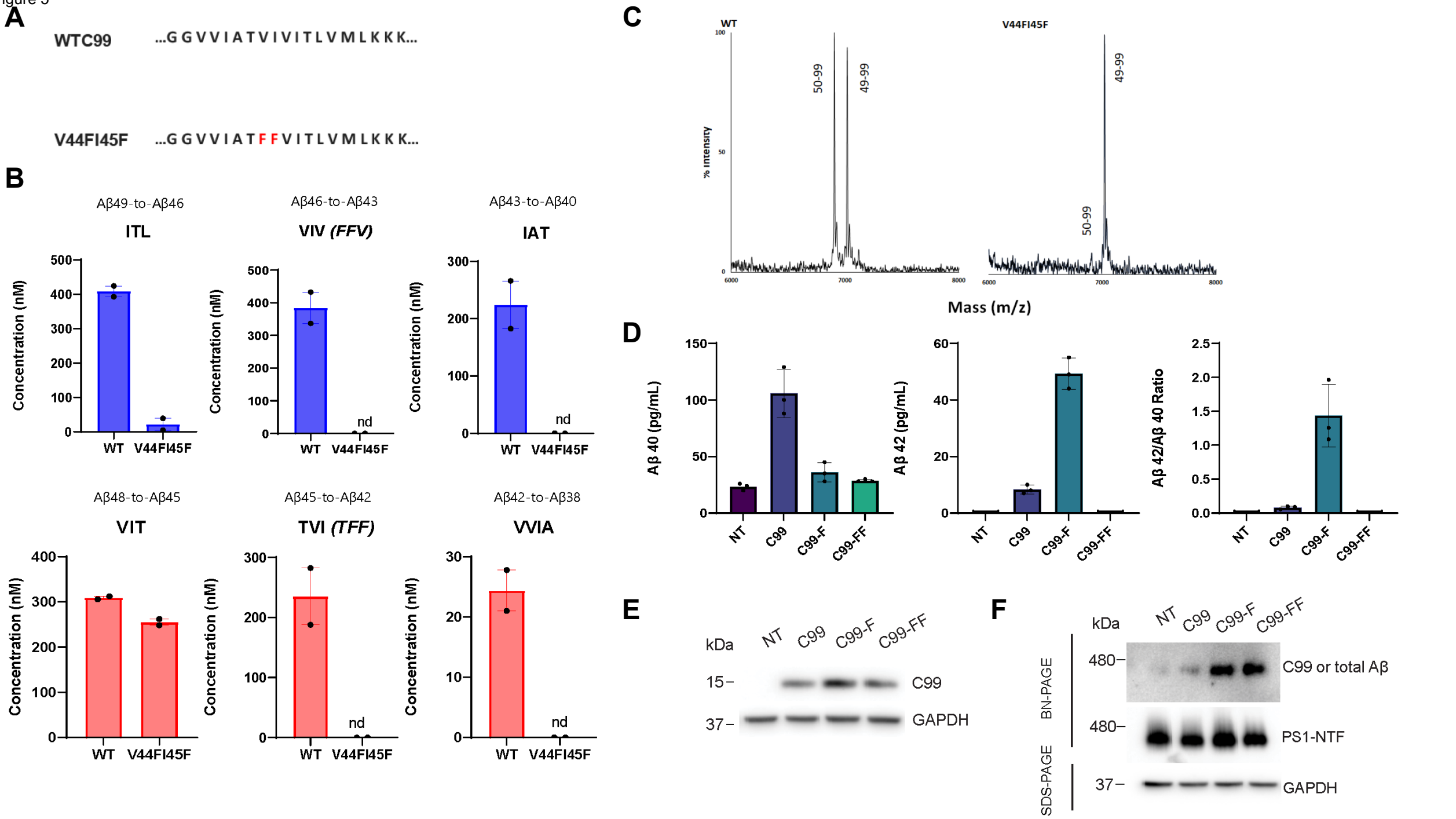
A
WTC99 ...G G V V I A T V I V I T L V M L K K K...
V44FI45F ...G G V V I A T F F V I T L V M L K K K...
B
Aβ49-to-Aβ46
ITL
Aβ46-to-Aβ43
VIV (FFV)
Aβ43-to-Aβ40
IAT
Aβ48-to-Aβ45
VIT
Aβ45-to-Aβ42
TVI (TFF)
Aβ42-to-Aβ38
VVIA
Concentration (nM)
WT
V44FI45F
nd
C
WT
V44FI45F
% Intensity
50-99
49-99
Mass (m/z)
D
Aβ 40 (pg/mL)
Aβ 42 (pg/mL)
Aβ 42/Aβ 40 Ratio
NT
C99
C99-F
C99-FF
E
kDa
15–
37–
C99
GAPDH
F
BN-PAGE
SDS-PAGE
480–
C99 or total Aβ
PS1-NTF
GAPDH

Figure 6

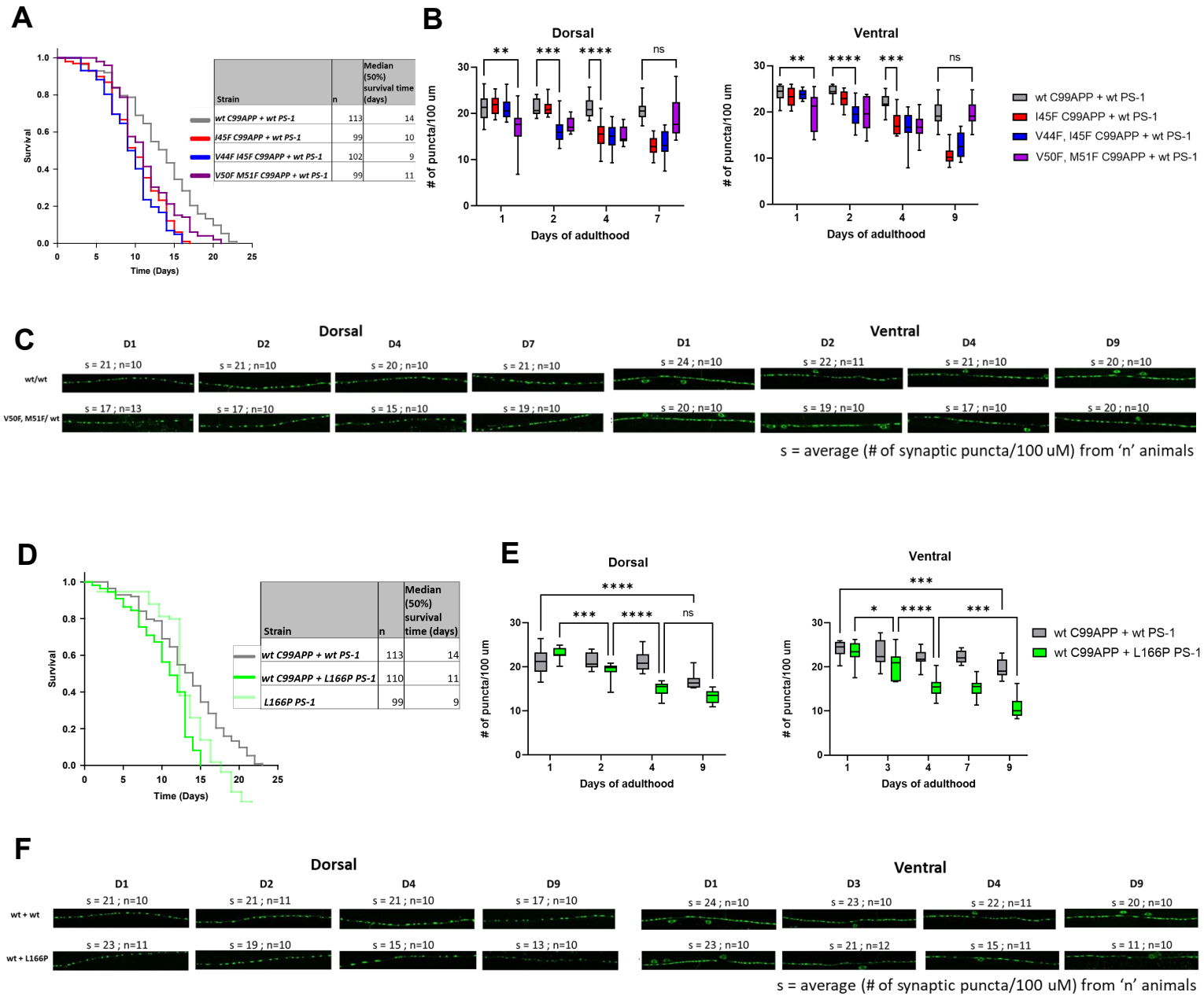
A
Survival
Time (Days)
Strain
n
Median (50%) survival time (days)
wt C99APP + wt PS-1
113
14
I45F C99APP + wt PS-1
99
10
V44F I45F C99APP + wt PS-1
102
9
V50F M51F C99APP + wt PS-1
99
11
B
Dorsal
Ventral
# of puncta/100 um
Days of adulthood
wt C99APP + wt PS-1
I45F C99APP + wt PS-1
V44F, I45F C99APP + wt PS-1
V50F, M51F C99APP + wt PS-1
C
Dorsal
Ventral
D1
D2
D4
D7
D9
wt/wt
V50F, M51F/ wt
s = 21 ; n=10
s = 17 ; n=13
s = 17 ; n=10
s = 15 ; n=10
s = 19 ; n=10
s = 24 ; n=10
s = 22 ; n=11
s = 21 ; n=10
s = 20 ; n=10
s = 19 ; n=10
s = 17 ; n=10
s = average (# of synaptic puncta/100 uM) from 'n' animals
D
Survival
Time (Days)
Strain
n
Median (50%) survival time (days)
wt C99APP + wt PS-1
113
14
wt C99APP + L166P PS-1
110
11
L166P PS-1
99
9
E
Dorsal
Ventral
# of puncta/100 um
Days of adulthood
wt C99APP + wt PS-1
wt C99APP + L166P PS-1
F
Dorsal
Ventral
D1
D2
D3
D4
D9
wt + wt
wt + L166P
s = 21 ; n=10
s = 21 ; n=11
s = 17 ; n=10
s = 23 ; n=11
s = 19 ; n=10
s = 15 ; n=10
s = 13 ; n=10
s = 24 ; n=10
s = 23 ; n=10
s = 22 ; n=11
s = 20 ; n=10
s = 21 ; n=12
s = 15 ; n=11
s = 11 ; n=10
s = average (# of synaptic puncta/100 uM) from 'n' animals

Figure 7

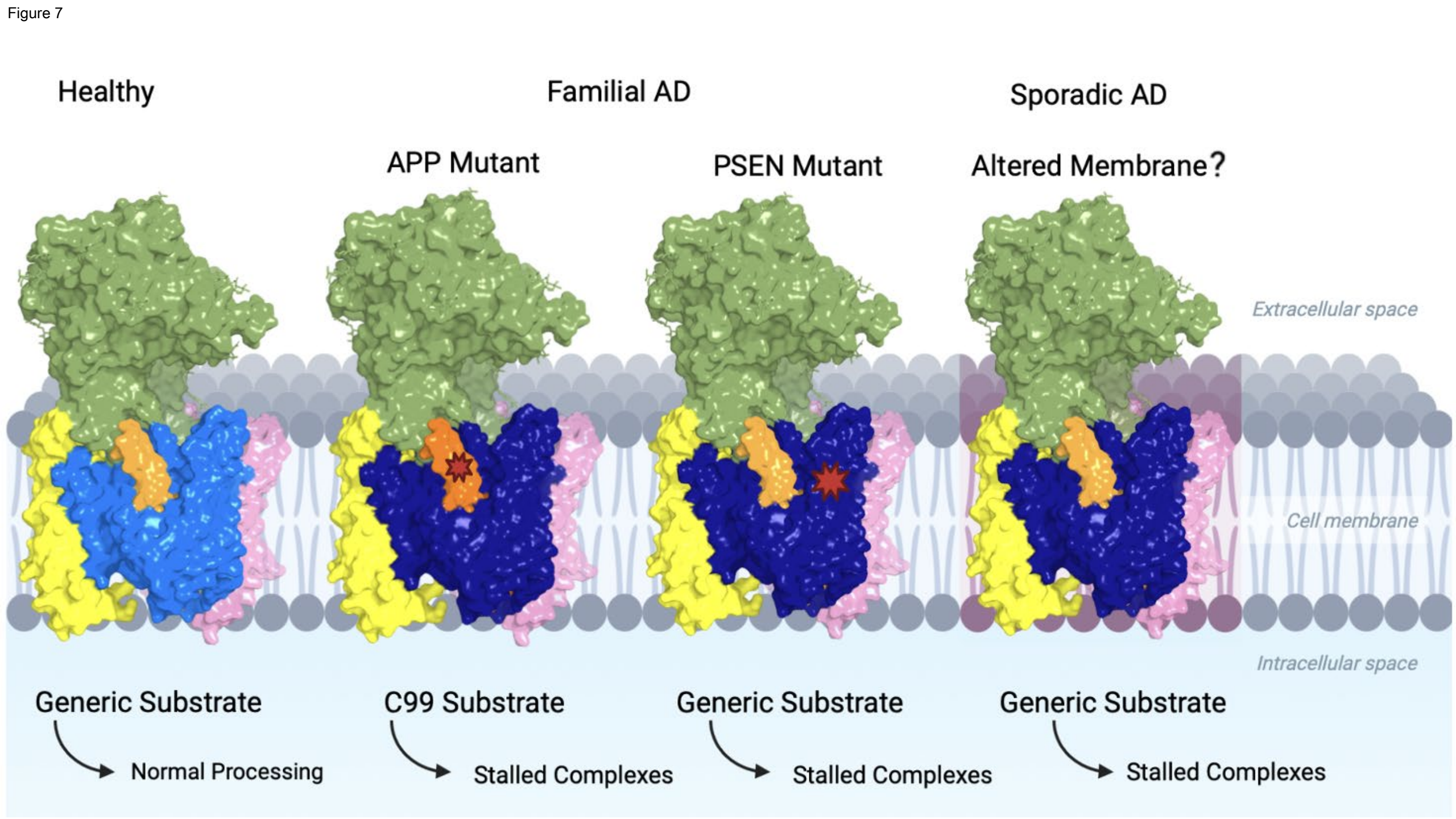
Healthy
Familial AD
Sporadic AD
APP Mutant
PSEN Mutant
Altered Membrane?
Extracellular space
Cell membrane
Intracellular space
Generic Substrate
Normal Processing
C99 Substrate
Stalled Complexes
Generic Substrate
Stalled Complexes
Generic Substrate
Stalled Complexes

Supplemental Information

Familial Alzheimer mutations stabilize synaptotoxic γ-secretase-substrate complexes

Sujan Devkota, Rui Zhou, Vaishnavi Nagarajan, Masato Maesako, Hung Do, Arshad Noorani, Caitlin Overmeyer, Sanjay Bhattarai, Justin T. Douglas, Anita Saraf, Yinglong Miao, Brian D. Ackley, Yigong Shi and Michael S. Wolfe

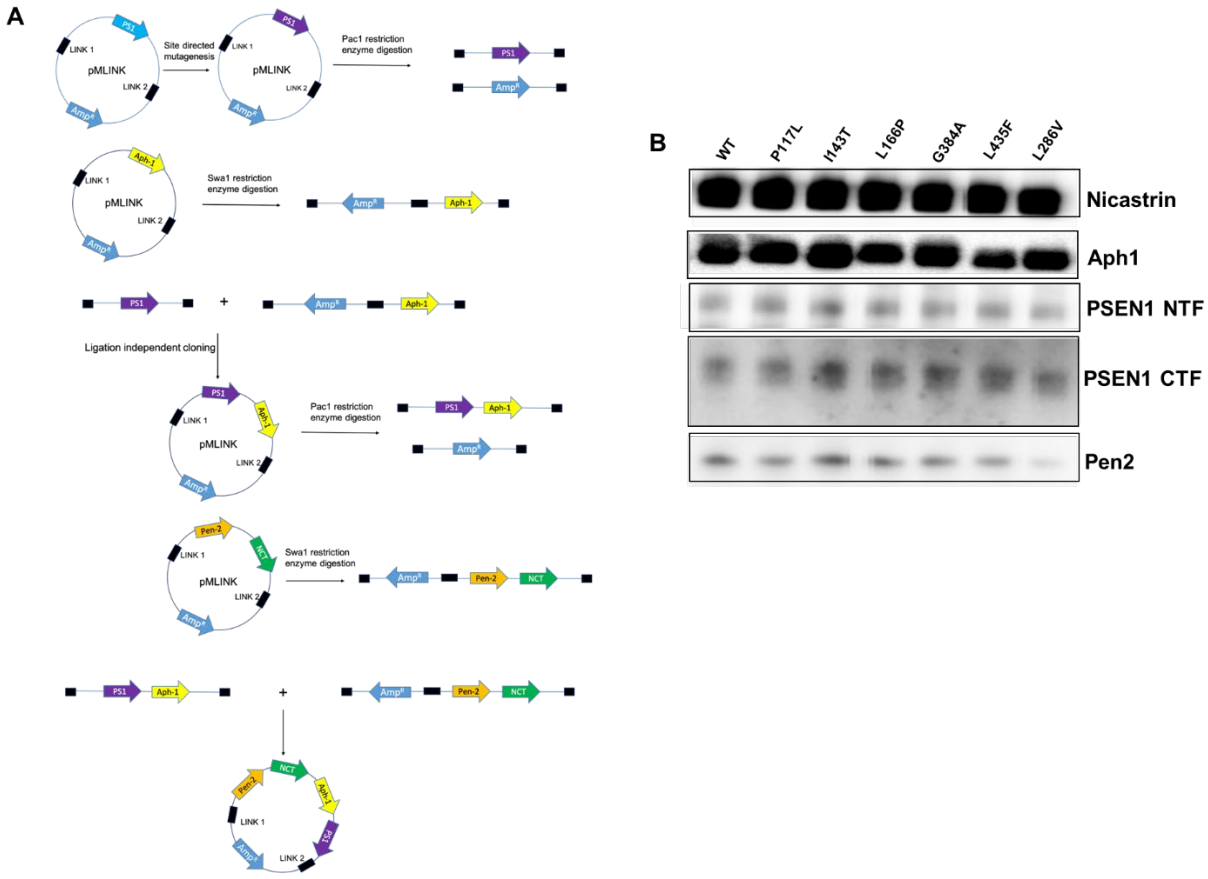

Figure S1. Generation and expression of pMLINK tetracistronic construct for FAD-mutant γ-secretase complexes. (A) FAD mutations were made in the PSEN1 coding region of pMLINK-PSEN1 by site-directed mutagenesis. FAD-mutant PSEN1 DNA was isolated after cleavage of Pac1 restriction sites in LINK1 and LINK2 regions. pMLINK-APhH1 was linearized via cleavage of a SwaI restriction site in LINK2. The PSEN1 fragment and linearized pMLINK-APhH1 were treated with T4 polymerase in the presence of dCTP or dGTP, respectively and combined by ligation independent cloning to create bicistronic pMLINK-Aph1-PSEN1 vector. Similarly, bicistonic pMLINK-Pen2-Nicastrin was created. Finally, the two bicistronic vectors were used to make the tetracistronic vector (pMLINK-PEN-2-nicastrin-APH-1-PS1). (B) Western blot of all components of expressed and purified WT and FAD-mutant γ-secretase complexes, normalized for protein concentration.

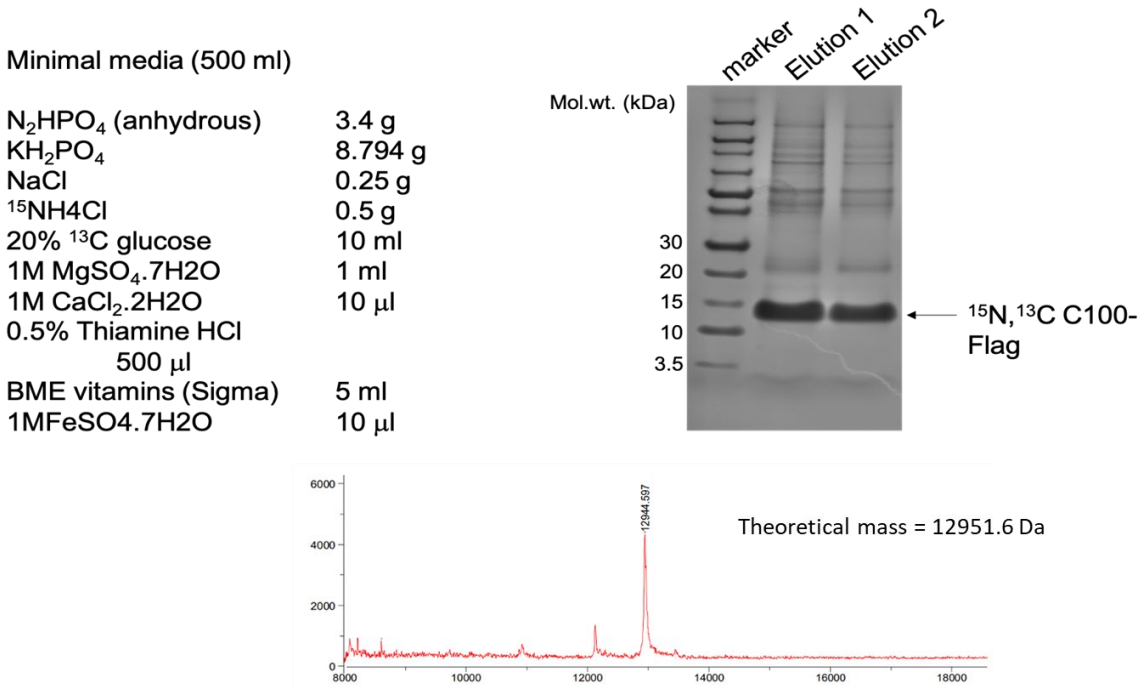

Figure S2. Production, purification and characterization of heavy isotopic C100Flag protein. *E. coli* BL21 cells were grown in minimal media with 20% ^{13}C glucose and $^{15}NH_4Cl$ (complete composition shown) and induced with 0.5 mM IPTG. Cell lysate was incubated with anti-FLAG M2-agarose beads, and C100-FLAG protein was eluted with 100 mM glycine buffer at pH 2.7 and 0.25% NP-40, followed by neutralization with pH 8 Tris buffer. The identity and purity of C100-FLAG was analyzed by SDS/PAGE with Coomassie staining and MALDI-TOF mass spectrometry. Note: Theoretical monotopic mass of light C100-FLAG is 12,265.05.

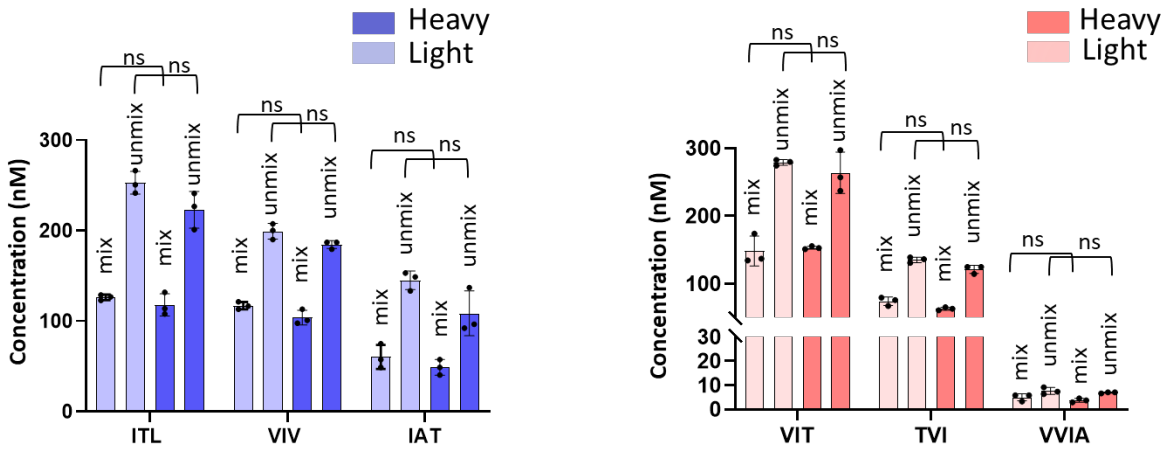

Figure S3. Validation of light- vs. heavy-isotopic substrate labeling method using WT γ-secretase. Light- and heavy-isotope labeled C100Flag substrate were separately incubated with WT γ-secretase. After quenching, the two enzyme reactions were then mixed 1:1 for analysis of small peptide co-products of each proteolytic event. Shown are the concentrations of each co-product for both the unmixed and mixed samples. Note that light- and heavy-isotope labeled substrate gives equimolar levels of each small peptide, both in the unmixed and mixed samples. Mixed samples contain half the light or heavy co-product seen in the unmixed samples due to the 1:1 dilution. N=3, unpaired two-tailed T-test

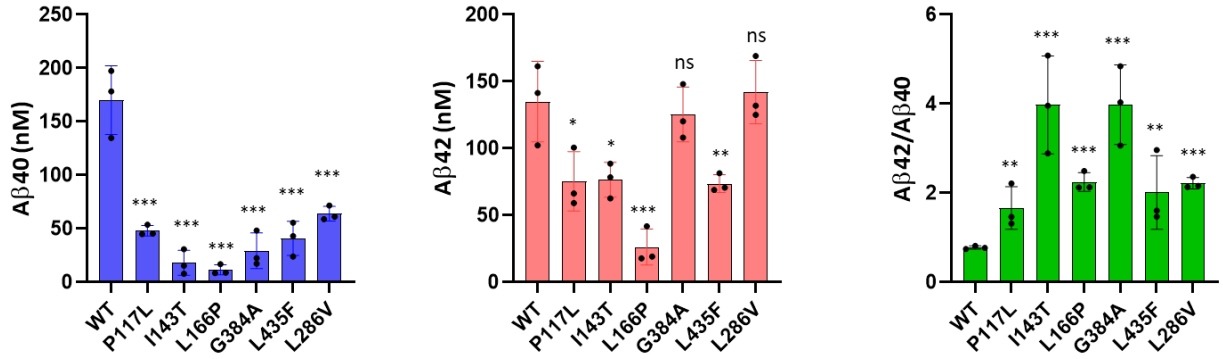

Figure S4. Aβ40, Aβ42, and Aβ42/Aβ40 ratio from cleavage of APP substrate by WT and FAD-mutant γ-secretases. Aβ40 and Aβ42 produced by incubation of purified γ-secretase and C100Flag, as determined by specific ELISAs, and the resulting Aβ42/Aβ40 ratios. N=3, unpaired two-tailed T-test of FAD mutants compared to WT, *p≤ 0.05, **p≤ 0.01, ***p≤ 0.001.

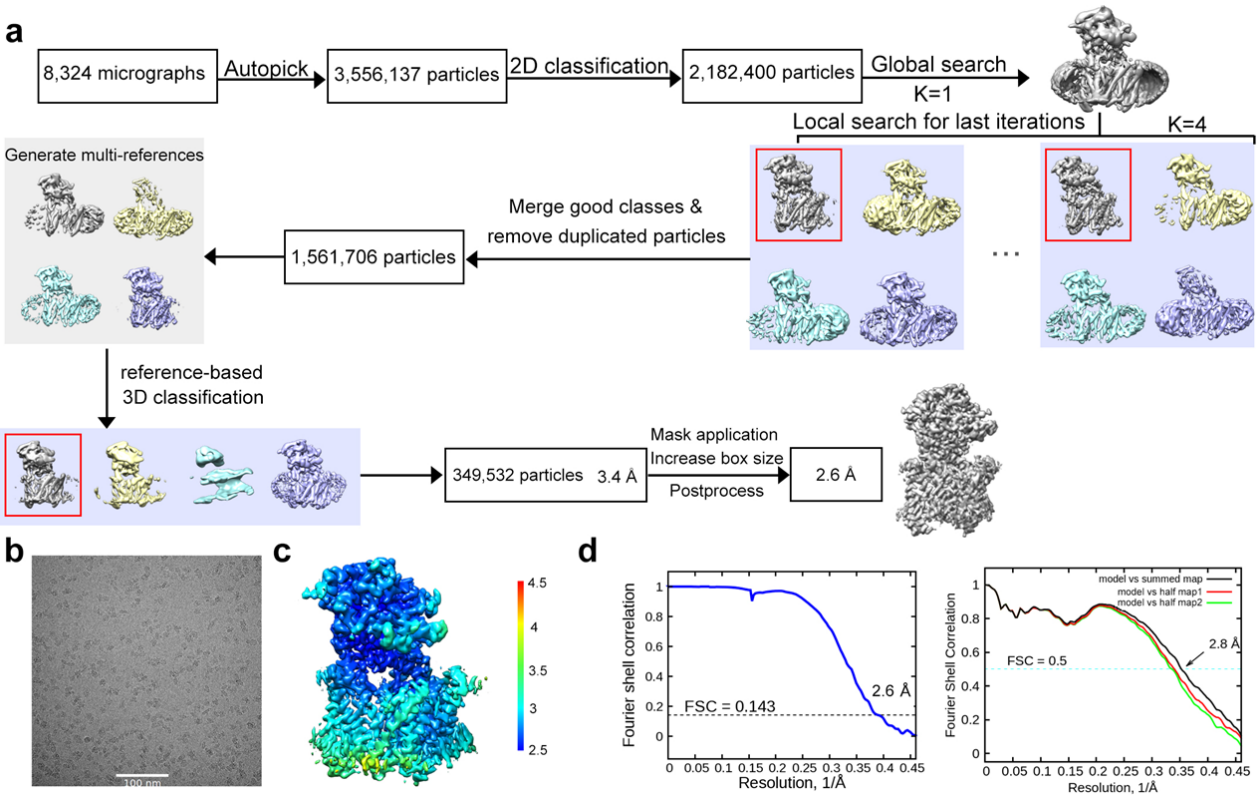

Figure S5. Cryo-EM analysis of SB-250 bound to human γ-secretase. (A) Flowchart of cryo-EM data processing. Please refer to STAR Methods for details. (B) Representative cryo-EM micrograph of SB-250 bound human γ-secretase. A scale bar of 100 nm is shown. (C) Color-coded local resolution distribution in Å of the final reconstruction, estimated by RELION-3.0. (D) The final average resolution of the reconstruction of SB-250 bound human γ-secretase is 2.6 Å based on the 0.143 FSC curve. (left panel) The FSC curves of the refined model versus the maps that it is refined against (black); the model refined in the first of the two independent maps used for the FSC calculation versus that same map (red); and the model refined in the first of the two independent maps versus the second independent map (green) (right panel). The small difference between the red and green curves indicates that the refinement did not suffer from overfitting.

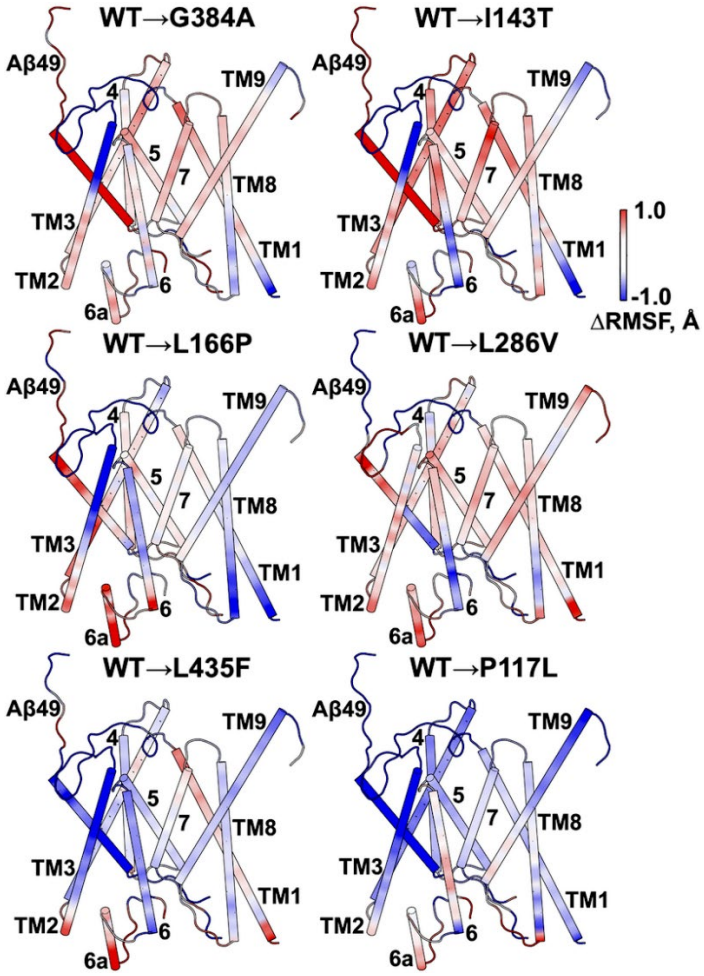

Figure S6. Molecular dynamics simulations of γ-secretase bound to Aβ49. Differences in RMSF between WT and FAD-mutant γ-secretase bound to Aβ49 show the FAD-mutant PSEN1 P117L leads to the most reduced conformational flexibility, especially for bound Aβ49, implying enzyme-intermediate complex stabilization.

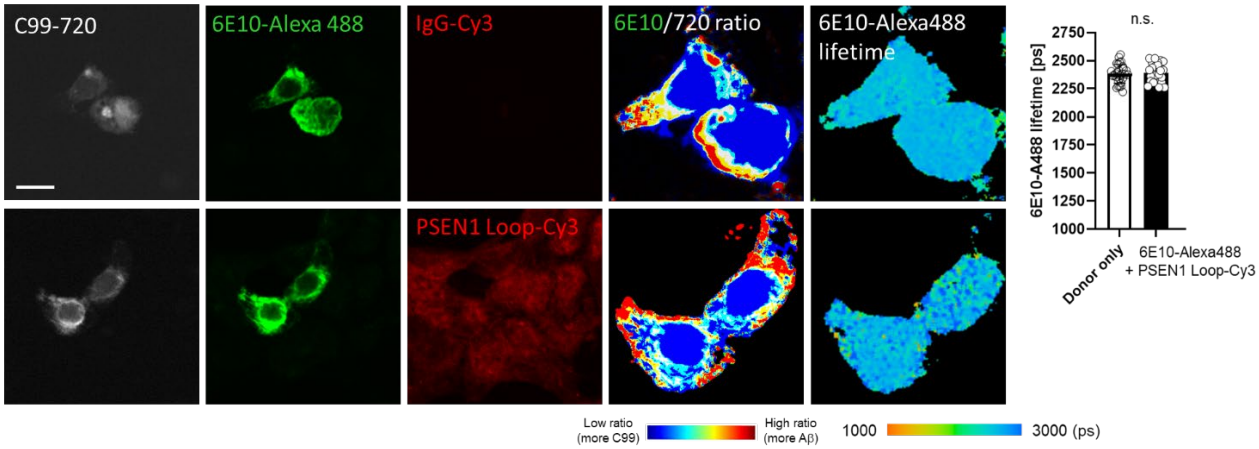

Figure S7. Control FLIM experiments using quencher-antibody that bind distal to 6E10 binding site on C99/Aβ. Specifically, rabbit monoclonal antibody EP2000Y to PSEN1 Loop was used in place of anti-nicastrin antibody NBP2-57365 used in main Fig. 3.

Table S1. Quantification of concentration (nM) of each Aβ product from processing of APP substrate by WT vis-à-vis FAD-mutant γ-secretase.[a]

PSEN1	Aβ49	Aβ48	Aβ46	Aβ45	Aβ43	Aβ42	Aβ40	Aβ38
WT	90	118	45	60	10	132	193	62
P117L	151	172	20	-7	20	28	24	16
I143T	9	32	22	0	0	*nd*	*nd*	*nd*
L166P	9	19	24	0	0	*nd*	*nd*	*nd*
G384A	46	126	20	-6	19	25	24	17
L435F	-5	29	28	0	0	*nd*	*nd*	*nd*
L286V	-8	35	33	21	44	62	80	26

[a]Calculation of concentration of each Aβ species produced by incubation of purified γ-secretase complexes and C100Flag, based on concentrations of co-products: [$Aβ_x$] = [co-product of $Aβ_x$ production] – [co-product of $Aβ_x$ degradation] (e.g., [Aβ49]=[AICD50-99]-[ITL]. Concentration of each Aβ species in nM produced from reaction mixtures of 3 μM of C100Flag by 30 nM WT or FAD-mutant γ-secretase incubated at 37 °C for 16 h. Where the net level of precursor Aβ peptide for a given trimming step is zero, the net level of the trimmed Aβ product was not determined (nd).

Table S2. Sum of Aβ product concentrations (nM) equal sum of AICD product concentrations (nM) from processing of APP substrate by WT vis-à-vis FAD-mutant γ-secretase.[a]

PSEN1	Total Aβ	Total AICD	Aβ40+Aβ43+ Aβ46+Aβ49	AICD 50-99	Aβ38+Aβ40+ Aβ45+Aβ48	AICD 49-99
WT	714	668	340	334	374	334
P117L	427	434	217	204	210	230
I143T	64	51	32	23	32	28
L166P	52	50	33	25	19	26
G384A	274	289	111	115	163	174
L435F	52	47	23	24	29	23
L286V	297	301	151	141	146	160

[a]Note total Aβ levels equal total AICD levels for each γ-secretase variant. Equimolar levels are also observed for Aβ peptides along the Aβ40 and Aβ42 pathways compared to corresponding AICD species (AICD50-99 and AICD49-99, respectively).

Table S3. Data collection and refinement statistics

	#1 name (EMDB-36948) (PDB 8K8E)
Data collection and processing	
Magnification	81,000
Voltage (kV)	300
Electron exposure (e–/Å^2)	50
Defocus range (μm)	~1.5-~1.8
Pixel size (Å)	1.0825
Symmetry imposed	C1
Initial particle images (no.)	3,556,137
Final particle images (no.)	349,532
Map resolution (Å)	2.6
FSC threshold	0.143
Map resolution range (Å)	2.5-4
Refinement	
Initial model used (PDB code)	6IYC
Model resolution (Å)	2.8
FSC threshold	0.5
Model resolution range (Å)	2.8-256
Map sharpening *B* factor (Å^2)	-10
Model composition	
Non-hydrogen atoms	10,856
Protein residues	1,324
Ligands	26
B factors (Å^2)	
Protein	101.20
Ligand	126.72
R.m.s. deviations	
Bond lengths (Å)	0.004
Bond angles (°)	0.621
Validation	
MolProbity score	1.98
Clashscore	7.36
Poor rotamers (%)	1.77
Ramachandran plot	
Favored (%)	94.30
Allowed (%)	5.70
Disallowed (%)	0.00

Table S4. Summary of Pep-GaMD simulations of WT and PS1 FAD mutant γ-secretase bound by Aβ49 substrate and AICD50-99.

System	Method	Simulation Length (ns)	Boost Potential (kcal/mol)
WT	Pep-GaMD_Dual	3 x 600	98.9 ± 10.9
P117L	Pep-GaMD_Dual	3 x 600	104.4 ± 11.3
I143T	Pep-GaMD_Dual	3 x 600	104.3 ± 11.7
L166P	Pep-GaMD_Dual	3 x 600	102.8 ± 11.4
G384A	Pep-GaMD_Dual	3 x 600	100.5 ± 11.1
L435F	Pep-GaMD_Dual	3 x 600	105.9 ± 11.8
L286V	Pep-GaMD_Dual	3 x 600	104.3 ± 11.5

Table S5. Survival curve analysis of *C. elegans* transgenic lines using data from experiments shown in main Figs 4 and 6.

Transgenic lines	Total # of worms (n)	Survival Time (Days)	Std. Error	Survival Time (Days)	Std. Error	Survival Time (Days)	Std. Error	Survival Time (Days)	Std. Error
		Mean		25th Percentile[a]		50th Percentile[b]		75th Percentile[c]	
Figure 4b									
wt C99APP + wt PS-1	113	13.274	0.476	17	0.611	14	0.659	10	0.867
I45F C99APP + wt PS-1	99	10.02	0.368	13	0.548	10	0.48	7	0.269
I45F C99APP	100	12.97	0.439	16	0.481	14	0.762	10	0.612
Figure 4e									
wt C99APP + wt PS-1	113	13.274	0.476	17	0.611	14	0.659	10	0.867
I45F C99APP + wt PS-1	99	10.02	0.368	13	0.548	10	0.48	7	0.269
V44F I45F C99APP + wt PS-1	102	9.51	0.335	11	0.408	9	0.404	7	0.422
V44F I45F C99APP	102	11.961	0.293	14	0.367	12	0.488	10	0.302
Figure 6a									
wt C99APP + wt PS-1	113	13.274	0.476	17	0.611	14	0.659	10	0.867
I45F C99APP + wt PS-1	99	10.02	0.368	13	0.548	10	0.48	7	0.269
V44F I45F C99APP + wt PS-1	102	9.51	0.335	11	0.408	9	0.404	7	0.422
V50F M51F C99APP + wt PS-1	99	11.343	0.377	14	0.814	11	0.613	9	0.378
Figure 6d									
wt C99APP + wt PS-1	113	13.274	0.476	17	0.611	14	0.659	10	0.867
wt C99APP + L166P PS-1	110	10.336	0.346	13	0.14	11	0.583	8	0.752
L166P PS-1	99	10.343	0.348	13	0.64	9	0.553	8	0.159

[a]Survival time where 75% of the animals are expected to survive. [b]median survival time. [c]survival time where 25% of the animals are expected to survive.

Table S6. Pairwise comparison of survival curves of *C. elegans* transgenic lines using data from experiments shown in main Figs 4 and 6.

Pairwise multiple comparison (Holm-Sidak method)	**Overall Significance level cutoff: <0.05**	
Comparisons	**P Value**	**Significant?**
Figure 4b		
wt C99APP + wt PS-1 vs *I45F C99APP + wt PS-1*	3.46E-09	Yes
I45F C99APP + wt PS-1 vs *I45F C99APP*	1.21E-08	Yes
wt C99APP + wt PS-1 vs *I45F C99APP*	0.151	No
Figure 4e		
wt C99APP + wt PS-1 vs *V44F I45F C99APP + wt PS-1*	1.43E-11	Yes
wt C99APP + wt PS-1 vs *V44F I45F C99APP*	0.000187	Yes
V44F I45F C99APP + wt PS-1 vs *V44F I45F C99APP*	2.31E-05	Yes
I45F C99APP + wt PS-1 vs *V44F I45F C99APP + wt PS-1*	0.211	No
Figure 6a		
wt C99APP + wt PS-1 vs *V50F M51F C99APP + wt PS-1*	0.00066	Yes
I45F C99APP + wt PS-1 vs *V50F M51F C99APP + wt PS-1*	0.0217	Yes
V44F I45F C99APP + wt PS-1 vs *V50F M51F C99APP +wt PS-1*	0.00092	Yes
Figure 6d		
wt C99APP + wt PS-1 vs *wt C99APP + L166P PS-1*	3.7E-09	Yes
wt C99APP + wt PS-1 vs *L166P PS-1*	1.8E-07	Yes
L166P PS-1 vs *wt C99APP + L166P PS-1*	0.823	No